Palaeogeography, Palaeoclimatology, Palaeoecology 589 (2022) 110818

Contents lists available at ScienceDirect

Palaeogeography, Palaeoclimatology, Palaeoecology

journal homepage: www.elsevier.com/locate/palaeo

A rapid sedimentary response to the Paleocene-Eocene Thermal Maximum hydrological change: New data from alluvial units of the Tremp-Graus Basin (Spanish Pyrenees)

Victoriano Pujalte [a,*], Birger Schmitz [b], Aitor Payros [a]

[a] Department of Geology, Faculty of Science and Technology, University of the Basque Country UPV/EHU, Bilbao, Spain
[b] Division of Nuclear Physics, Department of Physics, University of Lund, Lund, Sweden

ARTICLE INFO

Editor: A Dickson

Keywords:
Claret Conglomerate
CIE onset
PETM
Organic carbon isotopes

ABSTRACT

A massive emission of light carbon about 56 Ma, recorded in marine and terrestrial sediments by a negative carbon isotope excursion (CIE), caused a short-lived (~170 kyr) global warming event known as the Paleocene–Eocene Thermal Maximum (PETM). The onset and core of this event is represented in the south Pyrenean Tremp-Graus Basin by two successive alluvial units, the Claret Conglomerate (CC) and the Yellowish Soils, which represent laterally juxtaposed depositional environments. It is generally agreed that these units record a dramatic increase in seasonal rain and an increased intra-annual humidity gradient during the PETM, but the timing of the sedimentary response to this hydrological change is a matter of debate. Some authors maintain that the CC was developed during the early, most intense phase of the carbon emission, others that its formation lagged by 16.5 ± 7.5 kyr behind the onset of the PETM. The latter claim was mainly based on the assumption that in two sections of this basin, Claret and Tendrui, the onset of the CIE occurs 3 and 8 m below the base of the CC, respectively. Here we show that in some zones between these two sections the CC was not deposited and the Yellowish Soil unit rests directly and conformably on the underlying Esplugafreda Formation. New $\delta^{13}C_{org}$ data from this intervening zone provide evidence that the onset of the CIE is situated just ~1 m below the Yellowish Soils. In adjacent sections the CC erosional base cuts down deeper than 5 m, thus removing or obscuring the chemostratigraphically-defined base of the PETM. A tentative estimate based on averaged sedimentation rates indicates that ~3.8 kyr, or less, may have elapsed from the onset of the CIE to the arrival of PETM alluvium into the Claret-Tendrui study area, less than half of the lowest estimate of previous authors. Since the study area was situated about 15 km from the source area, our new estimate supports a rapid response of the sedimentary system to the hydrological change at the onset of the PETM.

1. Introduction

The long-term environmental impact of the ongoing global warming is a matter of great concern and debate. One of its predicted effects is an alteration of the hydrological cycle, because a warmer atmosphere can hold more moisture (Held and Soden, 2006). However, the timing of the sedimentary response to such environmental changes remains uncertain. One way to predict these effects is modelling (Deser et al., 2020). For example, the modelling of river behaviour by Simpson and Castelltort (2012, p.1134) showed that variations in water discharge likely transmit, and can even amplify, sedimentary signals to downstream archives. Examples from modern alluvial systems also indicate that the sedimentary reaction to large rainfall events can be nearly instantaneous. For instance, an exceptional rainstorm (locally >600 l/m^2) in the semi-arid southeast of the Iberian Peninsula caused a catastrophic flood on October 18, 1973 (Capel Molina, 1974), after which a small fan delta in the coastal village of La Rábita experienced a seaward progradation of up to 270 m (Fig. 1).

An alternative way to learn about the sedimentary response to global warming and concomitant changes of the hydrological cycle is the study of past analogues, such as the Paleocene–Eocene Thermal Maximum (PETM), a short-lived (~170 kyr) global warming event that increased Earth's temperature by ~5–8 °C about 56 Ma ago. It was caused by a massive injection of light carbon into the ocean-atmosphere reservoirs,

* Corresponding author.
E-mail addresses: victoriano.pujalte@ehu.eus (V. Pujalte), birger.schmitz@nuclear.lu.se (B. Schmitz), a.payros@ehu.eus (A. Payros).

https://doi.org/10.1016/j.palaeo.2021.110818
Received 12 May 2021; Received in revised form 21 December 2021; Accepted 22 December 2021
Available online 28 December 2021

which was recorded in marine and terrestrial deposits by a prominent negative carbon isotope excursion (CIE) (Koch et al., 1992; Sluijs et al., 2007; Zachos et al., 2008; McInerney and Wing, 2011). Hydrological changes induced by the PETM have been reported in numerous studies. For instance, this event caused abrupt changes in alluvial architecture in the Piceance Creek Basin, Colorado, (Foreman et al., 2012; Foreman, 2014) and the Uinta Basin, Utah (Plink-Björklund et al., 2014), as well as an alteration of the stacking pattern and type of paleosols in the terrestrial Big Horn Basin, Wyoming (Kraus et al., 2013, 2015). Increased influx of terrestrial clays attributed to intensified rainfall and runoff have also been reported from widely separated continental margins (Gibson et al., 2000; Schmitz et al., 2001; John et al., 2008; Handley et al., 2012; Slotnick et al., 2012), while a massive input of both fine- and coarse-grained siliciclastics temporarily halted a long-lasting carbonate deposition in shallow marine areas of the Pyrenees (Pujalte et al., 2016; Pujalte and Schmitz, 2019) and the Xigaze forearc basin of the Tibet (Jiang et al., 2021).

The Claret Conglomerate (CC) of the Tremp-Graus Basin (southern Pyrenees), the focus of this study, is another prominent and amply referenced case (Schmitz and Pujalte, 2003, 2007; Armitage et al., 2011, 2013; Foreman et al., 2012; Minelli et al., 2013; Foreman, 2014; Pancost, 2017; Colombera et al., 2017; Allen, 2017; Carmichael et al., 2017, 2018). However, the time relationship between the PETM hydrological change and the sedimentary response recorded by the CC has created some discussion. Schmitz and Pujalte (2007), for instance, suggested that the CC was accumulated during the first 10 kyr, or less, of the PETM, which implies a rapid sedimentary response. Instead, Domingo et al. (2009), Manners et al. (2013) and Duller et al. (2019) (henceforward referred to collectively as DMD 09–19), mainly based on the study of $\delta^{13}C_{org}$ of two sections (Claret and Tendrui, here named Claret road and T_{DMD}), concluded that the onset of the thermal event predated the CC by 16.5 ± 7.5 kyr and postulated a delayed response of the sedimentary system to the PETM hydrological change.

A first purpose of this paper is to address this discrepancy. To this end, a detailed field study has been carried out in an area situated to the west of Tremp (study area in Supplementary Fig. 1A). Eight reference Paleocene-Eocene boundary sections were studied and sampled, including the controversial Claret and T_{DMD} sections, and a detailed field mapping of their surroundings was undertaken with the aim of gaining a wider perspective. As a result, the internal architecture of the CC in this area has been documented for the first time, shedding new light on the development of the unit. In addition, an attempt is made to estimate the rate of the sedimentary change induced by the PETM hydrological change, as recorded by the arrival of PETM alluvial clastics to the study area.

2. Geological setting, stratigraphy and prior information

In early Paleogene times the Tremp-Graus Basin was situated in the southeastern part of the Pyrenean marine gulf, an *E*-W elongated embayment opening westwards into the Bay of Biscay at ~35°N palaeolatitude (Fig. 2A; Baceta et al., 2011; Pujalte et al., 2016). The eastern part of the basin was mostly infilled with terrestrial deposits (Fig. 2B), informally named "Garumnian" (Rosell et al., 2001) and formally Tremp Group (Cuevas, 1992; Pujalte and Schmitz, 2005; Pujalte et al., 2014). This Group is underlain by transitional deposits of the Maastrichtian Aren Sandstone Formation, overlain by the marine "Alveolina limestone" unit (Ilerdian = lower Ypresian), and interfingers to the west with lacustrine and shallow marine carbonates (Pujalte et al., 2014).

In the Tremp-Graus Basin the PETM interval was first identified by Schmitz and Pujalte (2003) in the Esplugafreda section, mainly based on analyses of $\delta^{13}C$ of soil carbonate nodules (Supplementary Figs. 2A, B). Ten years later Manners et al. (2013) studied the isotopic composition of dispersed organic carbon of bulk samples ($\delta^{13}C_{org}$) across the Paleocene-Eocene boundary (P-E) interval of this section, placing the PETM in the same position (Supplementary Fig. 2C).

In the present study area, situated about 10 km to the south of Esplugafreda and just west of the city of Tremp (Fig. 2B, Supplementary Fig. 1), the P-E boundary interval comprises four of the five lithostratigraphic units recognized at Esplugafreda (Fig. 2C), their characteristics being summarized below from older to younger.

The Esplugafreda Formation (Thanetian, ~350 m thick at Claret) is mostly made up of overbank red and variegated silty mudstones with irregular intercalations of channelized calcarenites and calcareous conglomerates. The red mudstones include soil carbonate nodules, *Microcodium* (submillimeter-sized monocrystalline prisms of calcite originated on roots of terrestrial plants; Klappa, 1978; Košir, 2004) and a whole range of gypsum facies, from rosettes and root-like molds to

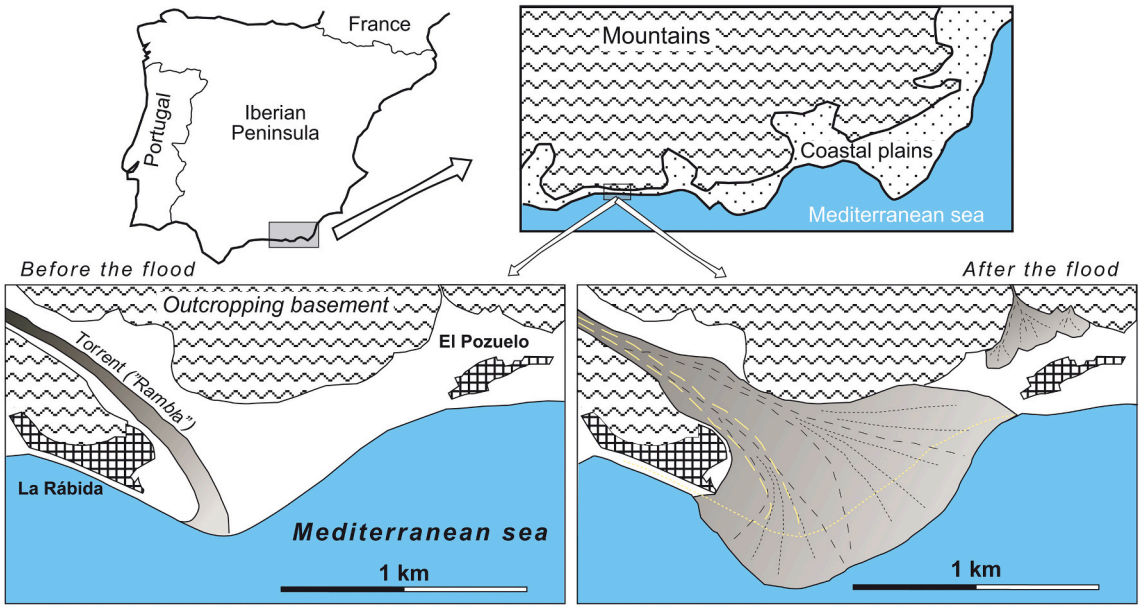

Fig. 1. Abrupt expansion (~270 m) of a small fan delta in the semiarid southeast coast of peninsular Spain during a single major flood (2580 m^3/seg at peak flow) after two days of heavy rain in October 1973. (For actual aerial images of the fan delta resulting from the flood visit: https://www.juntadeandalucia.es/institutodeestadisticaycartografia/blog/2015/07/el-tiempo-vuela-larabita/).

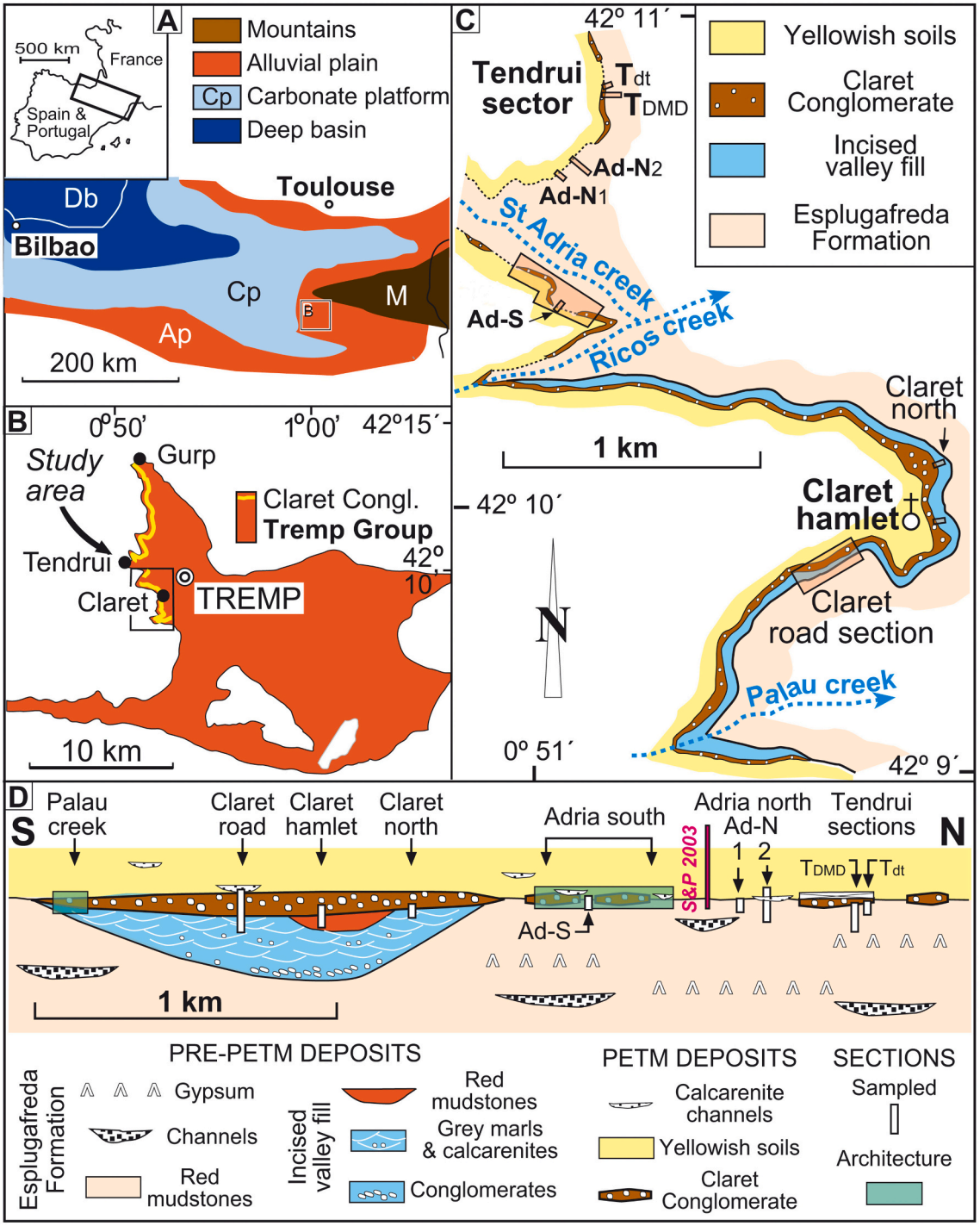

Fig. 2. (A) Simplified early Paleogene palaeogeography of the Pyrenean domain. (B) Outcrop map of the east part of the Tremp-Graus Basin with location of the study area. (C) Outcrop map of the Paleocene-Eocene interval in the study area. (D) Simplified S—N section (projected) showing the location of sections and outcrops described in the text (vertical scale exaggerated).

massive alabastrine accumulations up to 4 m thick, interpreted as deposits of ephemeral saline lakes (García Veigas, 1997), all of which provide evidence of semiarid to arid conditions.

In the study area the incised valley deposits infill an erosional depression ca. 1.5 km wide and up to 30 m deep excavated on the Esplugafreda Formation during a lowstand period predating the PETM (Fig. 2D; Pujalte et al., 2014). The lithological composition of this infill is markedly different to that of the Esplugrafreda Formation. It comprises coarse-grained imbricated conglomerates in its lower part that record westward flowing currents (Fig. 3A, B). The bulk of the unit, however, consists of alternating light grey calcarenites and marlstones devoid of carbonate nodules but rich in coalified remains, including occasional amber fragments, and even a root or small tree trunk buried in living position (Fig. 3C, D). The grey colours and abundant preservation of organic material are indicative of reducing conditions, probably in an aquatic/riparian setting. A minor but significant part of this unit consists of red mudstones with scattered soil carbonate nodules indicative of well-oxygenated conditions (Fig. 4A), their location attesting to the final infilling of the incised valley (Fig. 2D). Interestingly, the uppermost 30 cm of the red mudstones are intensely altered

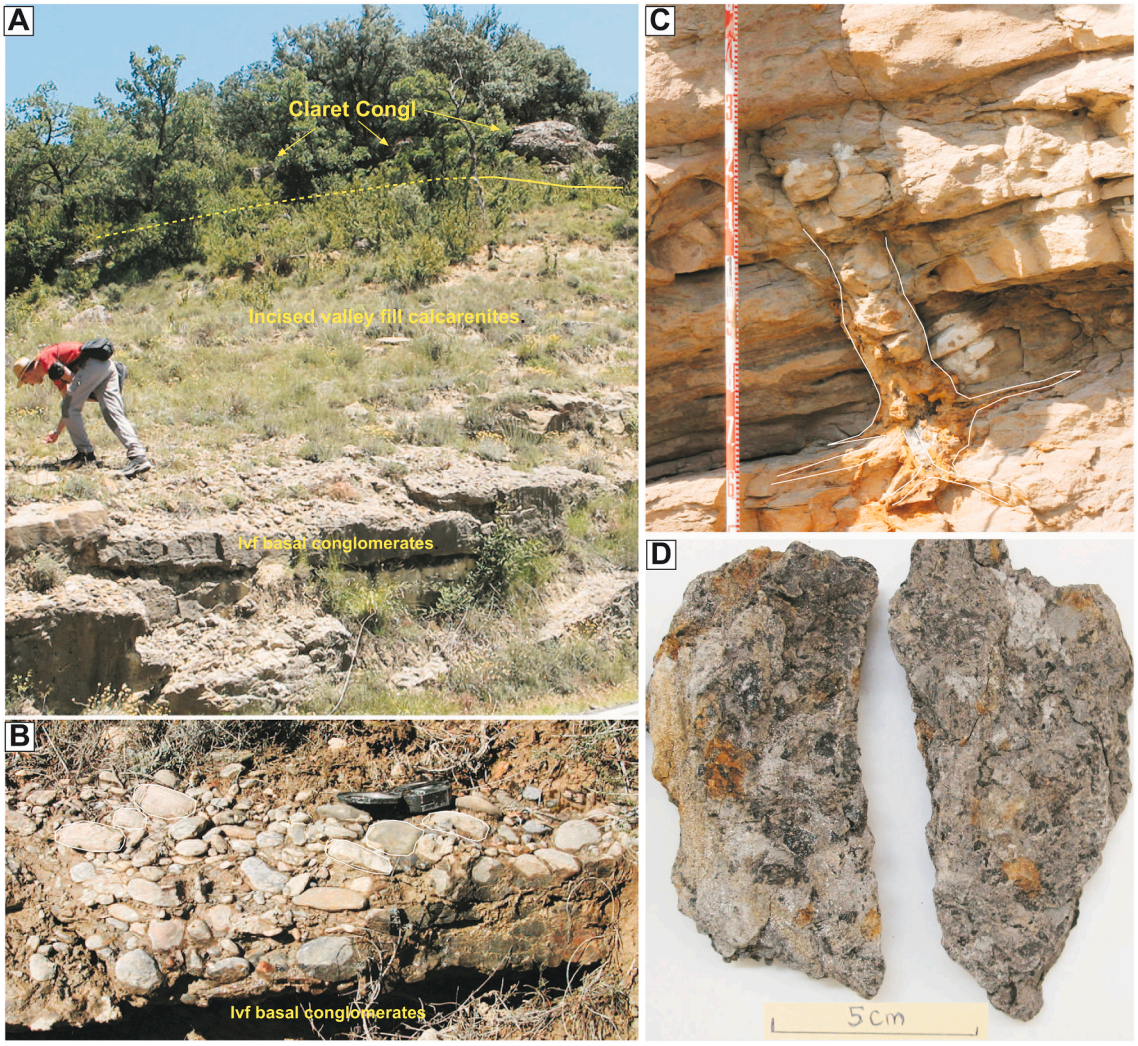

Fig. 3. Incised valley grey-coloured deposits at the Claret road section. (A) General view. (B) Close-up of the imbricated basal conglomerates of the valley fill. (C) Close-up of a root or small tree trunk buried in living position. (D) Abundant coal remains in a sample of the incised valley calcarenites.

(Fig. 4B). The altered zone contains abundant carbonate concretions that can be easily crushed and can hence be considered (sub)recent, an indication that the alteration was produced by hard waters percolating through the overlying CC. Alteration of sediments situated just below the CC has also been observed in other sections (e.g. Supplementary Fig. 3A).

In the Esplugafreda area (Supplementary Fig. 1A) the CC is laterally extensive unit up to 7 m thick of clast-supported calcareous conglomerates, pebbly calcarenites and minor mudstones (Schmitz and Pujalte, 2007). As described below, in the study area the CC is up to 4 m thick and has a discontinuous charater. The Yellowish Soils unit is up to 20 m thick and mainly consists of fine-grained mudstones of a light yellow colour in weathered exposures, with intercalated calcarenite channels 1–5 m thick but modest lateral extent (5–20 m). The mudstones contain abundant small-sized ($\leq$ 1 cm) soil carbonate nodules evenly distributed throughout the unit, but neither *Microcodium* nor gypsum have been observed. The Yellowish Soils generally overlie the CC but, according to Walther's Law of Facies, these two units probably represent frontally juxtaposed depositional environments, which implies that the CC grades distally into the Yellowish Soils.

The uppermost gypsum-rich unit is usually represented by red mudstones crisscrossed by gypsum veins and rosettes and locally by a 4 m thick package of massive alabastrine gypsum. In some sections this massive gypsum package is overlain by fresh-water limestones which yielded post-PETM $\delta^{13}C_{carb}$ values (Schmitz and Pujalte, 2003. Supplementary Fig. 3B).

Previous isotope records from soil carbonate nodules ($\delta^{13}C_{carb}$; Schmitz and Pujalte, 2003, 2007; Pujalte et al., 2014; Minelli et al., 2013) and from bulk dispersed organic matter in the Esplugafreda section ($\delta^{13}C_{org}$; Manners et al., 2013, Supplementary Fig. 2C) indicate that the Esplugafreda Formation and the incised valley fill deposits predate the PETM, the CC and the Yellowish Soils encompass the onset and core phases of the thermal event, while the recovery to pre-event background conditions is recorded in the gypsum-rich unit. However, the location of the base of the CIE in the study area is controversial. Schmitz and Pujalte (2003), Pujalte and Schmitz (2005) and Pujalte et al. (2009) placed it at the base of the CC, whereas DMD (09–19) maintain that it occurs below the CC, at about −3 m in the Claret section (here called Claret road; Fig. 2C) and − 8 m in the T_{DMD} section.

3. Material and methods

This study is mainly based on field observations, aided with satellite images of Google Earth and the Institut Cartogràfic i Geològic de Catalunya. The P-E boundary interval succession of the study area was remapped and the best outcrops photographed with a digital camera to facilitate the analysis of their facies and depositional architecture. Palaeocurrents were obtained from cross-bedding and the orientation of

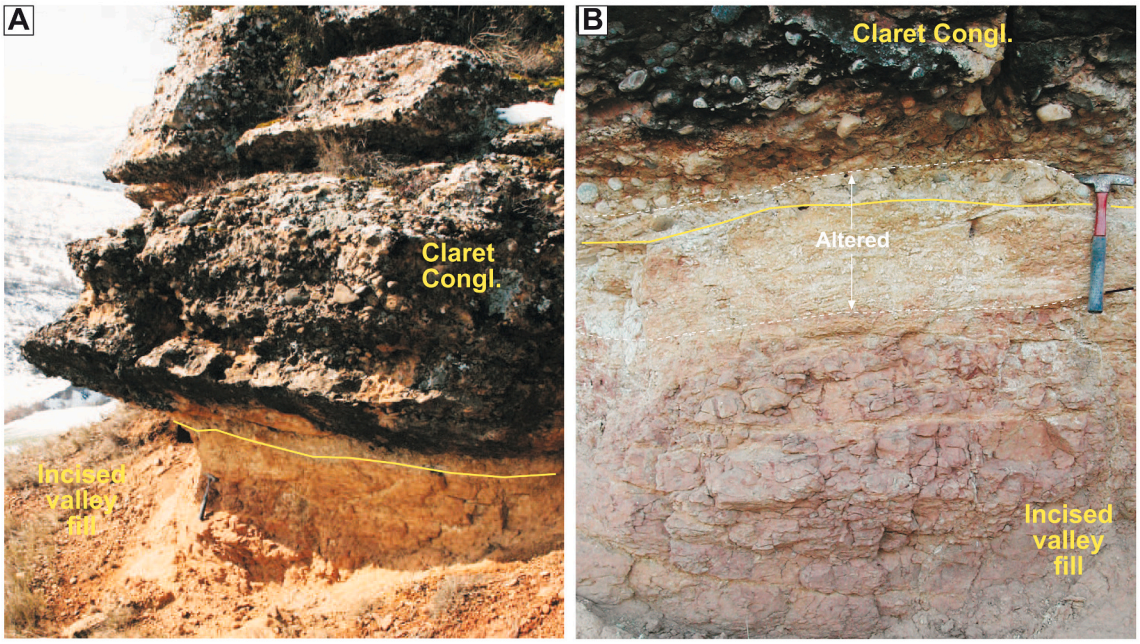

Fig. 4. (A) Incised valley red calcareous mudstones directly overlain by the Claret Conglomerate. (B) Close-up of the altered zone of the red mudstones directly below the Claret Conglomerate. (For interpretation of the references to colour in this figure legend, the reader is referred to the web version of this article.)

large scale dunes.

Nine sections have been studied in detail, six of them new. In eight of them 100 bulk samples were collected to analyze the isotopic composition of dispersed organic carbon, their coordinates and raw isotopic results being provided in the Supplementary Tables 1–8. The hardest pieces of the collected samples (i.e. the best preserved) were cleaned with distilled water to eliminate surface dust, dried at 30° in an oven for 24 h and finely ground on an agate mortar. The resulting powdered samples were analyzed for $\delta^{13}C$ of bulk dispersed organic matter at the Servizos de Apoio á Investigación (SAI) of the University of A Coruña, Spain. In three sections two analyses per sample were carried out. Powdered samples were weighed in silver capsules and decarbonated using 25% HCl at the Servizos de Apoio á Investigación (SAI) of the University of A Coruña, Spain. Measurements of stable isotope ratios were performed using a continuous-flow isotope-ratio mass spectrometer Deltaplus (Thermo Finnigan) coupled to an elemental analyzer FlashEA1112 (ThermoFinnigan) through a Conflo II interface (ThermoFinnigan). During analysis a set of international reference materials (USGS 40 (−26.39‰), USGS41a (+36.55‰), NBS 22 (−30.031‰), and USGS24 (−16.049‰) were analyzed for δ13C calibration. An analytical measurement error of ±0.15‰ (1 σ, $n = 10$) was obtained from replicate assays of the laboratory standard acetanilide interspersed between samples. Carbon isotope values are expressed relative to international standard VPDB (Vienna Pee Dee Belemnite).

In addition, previously published $\delta^{13}C_{carb}$ isotopic data from Schmitz and Pujalte (2003), Pujalte et al. (2009) (Supplementary Fig. 3B) and $\delta^{13}C_{org}$ isotopic data from DMD (09–19) have been reassessed.

4. Results

The CC is discontinuously developed in the study area, probably due to its relatively distal location (~15 km to the south of the source area, Supplementary Fig. 1A). When the CC is absent, the Esplugafreda Formation is directly overlain by the Yellowish Soils (Fig. 2C, D). Consequently, the P-E boundary interval successions present some significant differences in the Claret and Tendrui sectors, as well as in the intervening St Adria valley. These three zones are described separately below.

4.1. The P-E boundary interval in the Claret sector

The CC stretches for about 1.5 km in an N-S transect of the Claret sector, from the Palau creek in the south to the Ricos creek in the north, almost everywhere overlying the incised valley deposits (Fig. 2C, D). Due to its weathering resistant nature, the CC has created a cuesta landform, the top surface of which is widely exposed on the west-dipping gentle slope. This surface is generally sharp and nearly flat and is crisscrossed by a conspicuous conjugate set of joints, clearly noticeable in satellite images (Supplementary Figs. 4A, B). In turn, the CC has created a small cliff in the cuesta steep slope (Supplementary Fig. 4D).

Four sections have been studied in this sector, three of which were sampled (Fig. 2D). The Claret north, Claret hamlet and Palau sections are illustrated in Figs. 5 and 6 and briefly described below. The fourth one, the Claret road section, is dealt with in more detail in the next point, both to clarify the position of the base of the CIE and because it provides important clues about the internal architecture and development of the CC.

4.1.1. The Claret north, Claret hamlet and Palau sections

In the Claret north section, which is oriented nearly perpendicular to palaeocurrents (Fig. 5A), the CC is about 4 m thick and it is made up of stacked tabular packages of clast-supported conglomerates and lesser amounts of pebbly sandstones delimited by erosional surfaces (Fig. 5B). The lower boundary of the CC is sharp and slightly erosional, cutting ~60 cm into well exposed grey calcarenites and marlstones of the incised valley fill. The Palau creek section offers a NE-SW oriented vertical exposure, near parallel to palaeocurrents, in which large-scale unidirectional cross-bedding can be observed (Fig. 5C). Taken together, these two sections permit a 3D reconstruction of the internal architecture of the unit, providing a first indication of its south-westwards progradation.

The incised valley fill deposits situated just below the CC were analyzed for organic carbon isotopes in the Claret north and Claret hamlet sections (Fig. 6). The former exposes ~2 m of grey calcarenites and marls, from which 14 samples were collected at close-spaced intervals. The lower 10 samples provided a vertical stable trend, with $\delta^{13}C_{org}$ values ranging between −22 and − 23.6‰ (in black in Fig. 6A).

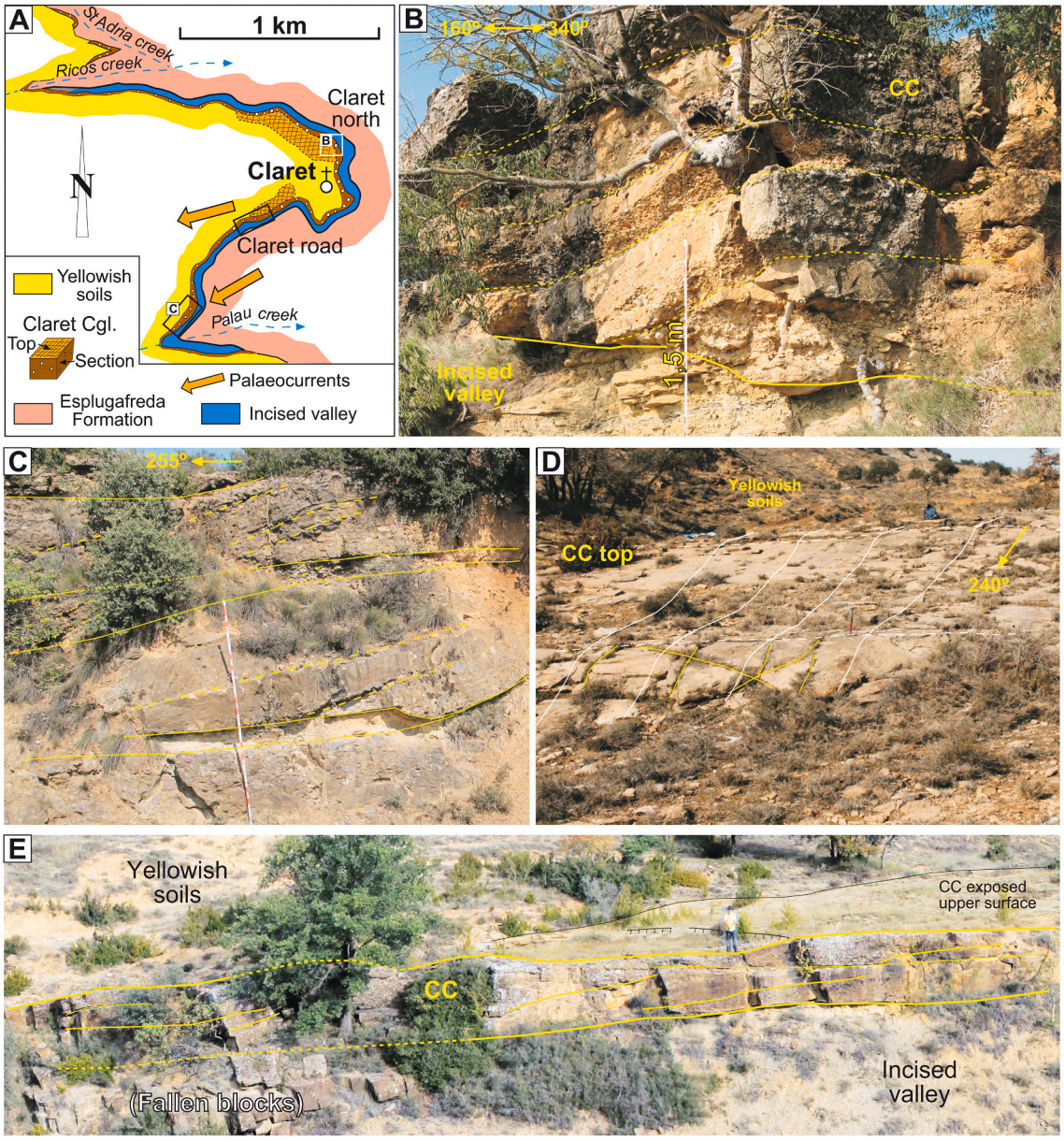

Fig. 5. (A) Outcrop map of the Paleocene-Eocene boundary deposits in the Claret sector with indication of palaeocurrents and location of the Claret north, Claret road and Palau creek sections. (B) Close-up of the Claret north section; note its orientation near perpendicular to palaeocurrents. (C) Close-up of part of the Claret road section showing cross-bedding in the Claret Conglomerate. (D, E) Two views of the Claret Conglomerate in the Palau creek section, respectively illustrating large-scale dunes on the top surface of the unit and large-scale cross-bedding in the vertical section.

Three out of the upper four samples, collected in the 20 cm interval situated just below the CC, also yielded low values (−22.7 to −24.2‰), the remaining one being somewhat more negative (−25.2‰; red in Fig. 6A; Supplementary Table 1).

In the Claret hamlet section the CC is underlain by about 5 m of red calcareous mudstones with scattered soil carbonate nodules. $\delta^{13}C_{org}$ values from four bulk samples of the red mudstones gave values between −24.4 and − 23.9‰ (Fig. 6B; Supplementary Table 2). In this same section Pujalte et al. (2009) reported the $\delta^{13}C_{carb}$ values of three nodules samples, respectively −7.3, −7.6 and − 7.7‰ (Supplementary Fig. 3B).

4.1.2. The Claret road section

The P-E boundary interval of the Claret road section is exposed in the trench of the road C-1311 from Tremp to the Montllobat Pass, near km 22. Due to its easy access it is the most studied and referenced section of the Claret sector (Pujalte and Schmitz, 2005; Pujalte et al., 2009; Domingo et al., 2009; Minelli et al., 2013; Manners et al., 2013; Pujalte and Schmitz, 2014; Payros et al., 2016; Duller et al., 2019). However, a major problem with this section is that the boundary between the incised valley deposits and the CC is not exposed, as it is covered up by a dense thicket of bushes and trees (Fig. 7A, Supplementary Fig. 5A). To overcome the problem, the scattered outcrops of the CC within the thicket were mapped in this study and connected with the road exposure. The uppermost incised valley stratum exposed in the road is a ~ 1 m thick calcarenite bed ("reference calcarenite"), the CC base being situated about 2 m above it (Fig. 7B, C). Between the reference calcarenite and the CC base vegetation and a thick recent soil preclude digging out fresh samples.

The CC is well outcropped in the road trench to the west of the thicket, but the underlying incised valley deposits are not exposed therein (Fig. 8). The CC is mainly composed of calcareous conglomerates and pebbly calcarenites, but it also contains sizable intercalations of

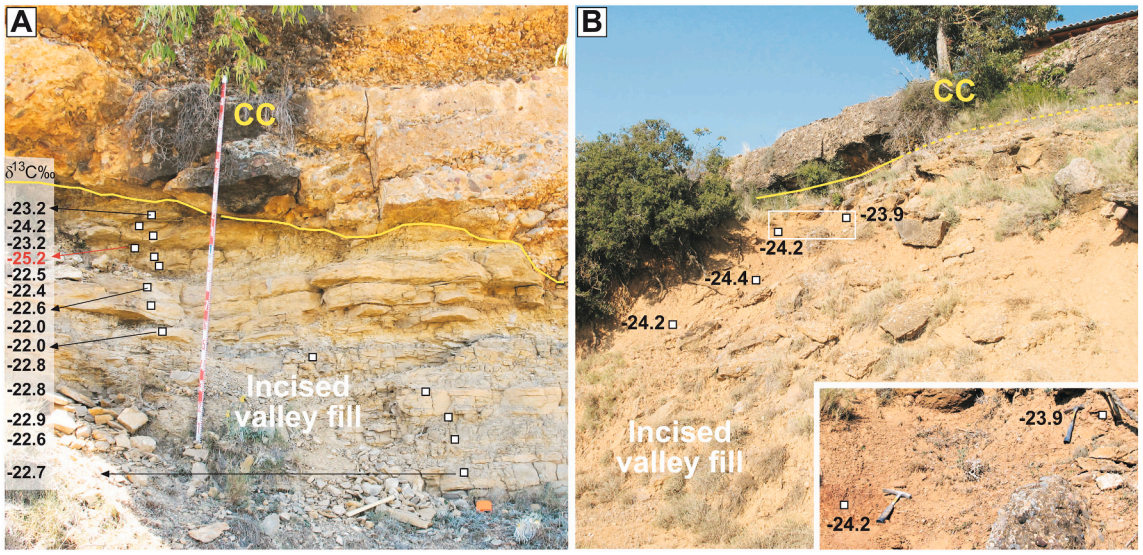

Fig. 6. Close up views and $\delta^{13}C_{org}$ values from the topmost part of the incised valley fill deposits of the Claret north (A) and the Claret hamlet (B) sections. Explanation within the text.

marly clays. Cross-stratifications in some of the conglomeratic beds consistently indicate west-directed palaeocurrents (Fig. 8), which demonstrates that the road trench provides a near dip oriented view of the CC. A large scale low-angle cross-stratification of the CC coarse beds is also evident, which denotes a westward progradation of the unit (Fig. 8A).

Pinpointing the top of the CC in the road trench itself is difficult because the unit is there directly overlain by one of the younger calcarenite channels intercalated in the Yellowish Soils. However, the near flat upper surface of the CC is widely exposed just north of the road, being readily recognizable by its tell-tale conjugate set of joints (Fig. 7A, Supplementary Figs. 5B, C). Tracing this surface to the road trench demonstrates that the alleged CC base in DMD (09–19) is actually situated only about 1 m below the top of the unit (Fig. 8A, Supplementary 5D). This circumstance inescapably demands that the samples collected by DMD (09–19) ~3 m below their CC base, which provided PETM values, must have been taken from marly clays intercalated within the CC, as indicated by Pujalte and Schmitz (2014).

We collected six samples for organic carbon isotope analysis in this section, three from the incised valley deposits and three from the marly clays intercalated in the CC conglomerates (Figs. 7C, 8A). Samples of the incised valley fill provide $\delta^{13}C_{org}$ values between −23.1 and −23.6‰, whereas those of the CC range between −25.3 and −26.1‰, averaging out at −25.6‰ (Supplementary Table 3).

4.2. The P-E boundary interval in St Adria valley

The St Adria creek has excavated a narrow valley that in its lower reach is about 80 m deep and exposes the entire Paleocene-Eocene boundary interval in both of its steep margins (Fig. 2C). The CC is discontinuous and only occurs on the southern margin (Fig. 2C). When the CC is absent the uppermost part of the Esplugafreda Formation consists of red silty marls with abundant $CaCO_3$ soil nodules capped by a 30–50 cm thick horizon of non-calcareous clays of a conspicuous purple colour, here named "purple cap" (Fig. 9A). This horizon is devoid of carbonate nodules but contains numerous small diameter ($\leq$ 1 mm) ferruginous nodules, their soft nature entailing an in situ origin (Fig. 9B). This purple cap, which was found in every accessible outcrop of the St Adria valley in which the CC is absent, is directly and conformably overlain by the Yellowish Soils.

Two separate CC packages are observable on the southern margin of the valley, both of them almost entirely encased within the Esplugafreda Formation (Fig. 10A, B). The one situated to the WNW is about 150 m wide and 2 m thick (Fig. 10B). In the zone between both CC packages a section, coded Ad-S, was sampled at close-spaced intervals across the Esplugafreda/Yellowish Soils transition (Fig. 10C, D; Supplementary Table 4). The five samples situated between −230 and −140 cm below the boundary gave a narrow range of $\delta^{13}C_{org}$ values (from −22.3 to −22.7‰). However, between −1 m and the Esplugafreda/Yellowish Soils boundary, $\delta^{13}C_{org}$ values became gradually more negative, first slowly and then rapidly, peaking at a minimum of −28.5‰ in the purple cap (Fig. 10C). Values of five samples analyzed from the overlying Yellowish Soils remain quite negative, ranging between −24.9 and −26.6‰.

The Esplugafreda/Yellowish soil boundary is also well exposed to the west of the WNW termination of the CC, except where a calcarenite channel intercalated in the Yellowish locally impinges on the Esplugafreda Formation (Fig. 10E). Below both the CC and the calcarenite channel, the purple cap has been eroded away.

On the northern margin of the St Adria valley the Yellowish Soils unit generally rests directly on the Esplugafreda Formation, as the CC is there absent. Two sections from this margin were analyzed, coded Ad-N_1 and Ad-N_2, respectively (Fig. 11A). A reduced purple cap is discernible in the former (Fig. 11B). In the upper 2.75 m of the Esplugafreda Formation, which have a similar composition to that in the AD-S section, including abundant carbonate nodules (Fig. 11C), seventeen mudstone samples were collected for organic carbon isotope analysis. Values of the lower thirteen of these samples vary between −22.3 and − 23.4‰, averaging out at −22.7‰, but in the uppermost 0.5 m of the Esplugafreda Formation values gradually decrease, peaking at −25.8‰ in the purple cap (Fig. 11B; Supplementary Table 5).

The Ad-N_2 section encompasses the uppermost 30 m of the Esplugafreda Formation, which are composed of alternating grey gypsiferous marls and red and variegated mudstones rich in carbonate nodules. The top of the Esplugafreda Formation is abruptly truncated by a 2 m thick calcarenite channel, in turn overlain by the Yellowish Soils (Fig. 11A, D). The $\delta^{13}C_{org}$ values throughout the Esplugafreda Formation are quite stable, varying between −23 and − 24‰ and averaging out at 23.5‰. A more negative value (−27‰) is recorded in the calcarenite channel, the negative values (−26‰) persisting within the overlying Yellowish Soils (Fig. 11D; Supplementary Table 6).

Schmitz and Pujalte (2003) sampled at low resolution another section of the St Adria northern margin situated about 200 m to the WNW of the Ad-N_1 section (S&P 2003 in Fig. 2D). The exposed part of the

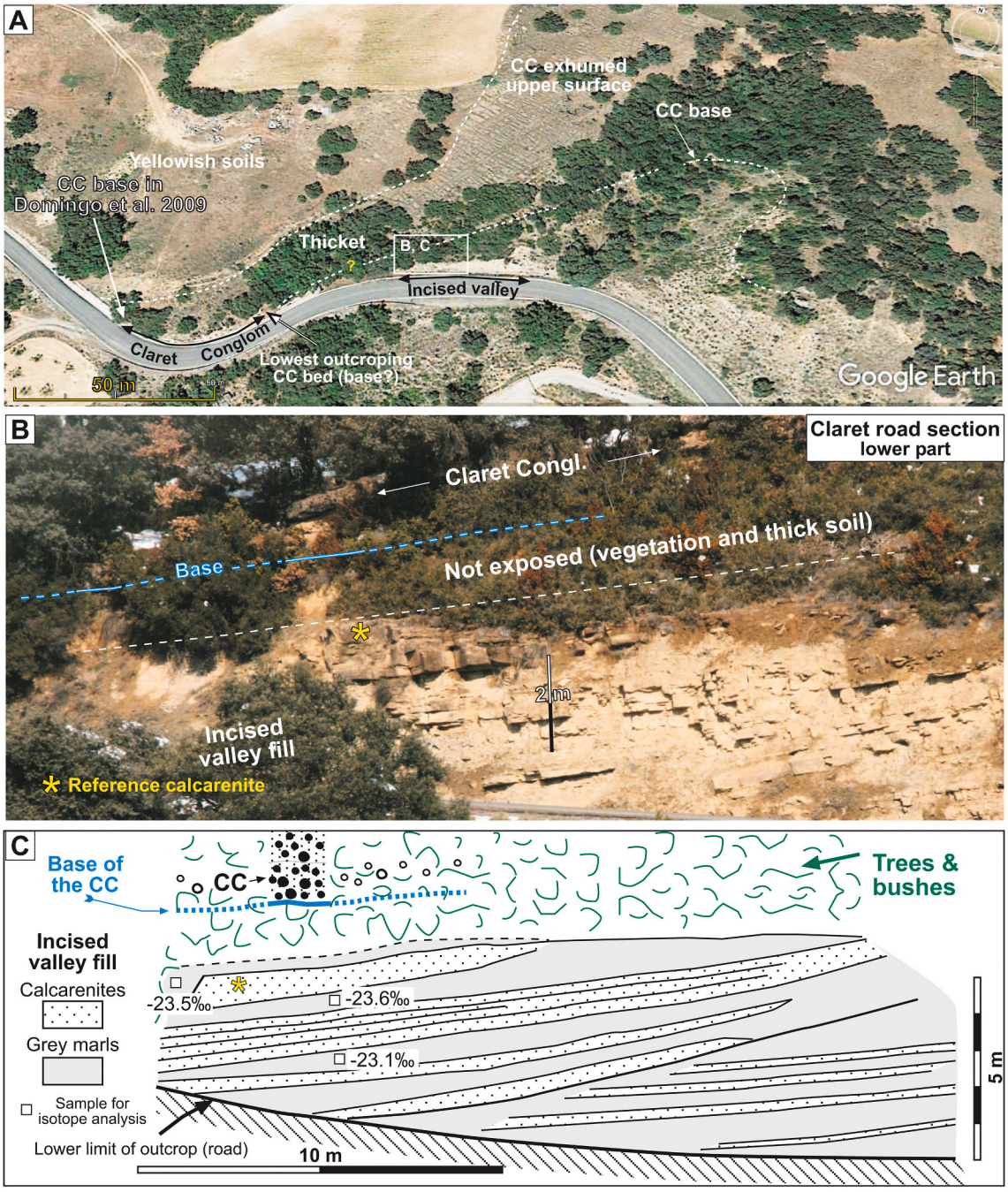

Fig. 7. (A) Map of the base and top of the CC drawn on a Google Earth satellite image of the area surrounding the Claret road section. Note that the CC base is hidden by vegetation throughout. (B, C) Field view and sketch of the upper part of the incised valley deposits, the poorly exposed CC and the intervening covered interval (location in A). Values of $\delta^{13}C_{org}$ isotopes from incised valley deposits are indicated in the sketch.

Esplugafreda Formation successively comprised grey marls with gypsum, red mudstones with carbonate nodules and the purple cap. Only one nodule sample was collected from the red marls, which produced a $\delta^{13}C_{carb}$ value of −8.6‰, whereas values of seven nodule samples from the Yellowish Soils varied between −12 to −14‰ (Supplementary Fig. 3B).

4.3. The P-E boundary interval in the Tendrui sector

The CC is about 1–3 m thick and stretches for about 265 m in S—N direction in the Tendrui sector, where it rests on the Esplugafreda Formation. It is overgrown with trees that prevent a proper assessment of its internal geometry. Neither can the nature of the sediments overlying the unit be established, as a farmland exists just above it (Figs. 11A, 12; Supplementary Fig. 6).

Field observations indicate that in the Tendrui sector the CC is entirely encased within the Esplugafreda Formation. This relationship can be visually deduced from the southern termination of the CC, but the encasement depth cannot be calculated because of the farmland on top of the CC (Fig. 11A). However, a cross-section across this southern part of the outcrop, in which the position of key horizons across the farmland has been extrapolated, supports that the top of the CC is situated below the top of the Esplugafreda Formation (Supplementary Fig. 6). Likewise, field relationships in the northern part of the outcrop confirm that that

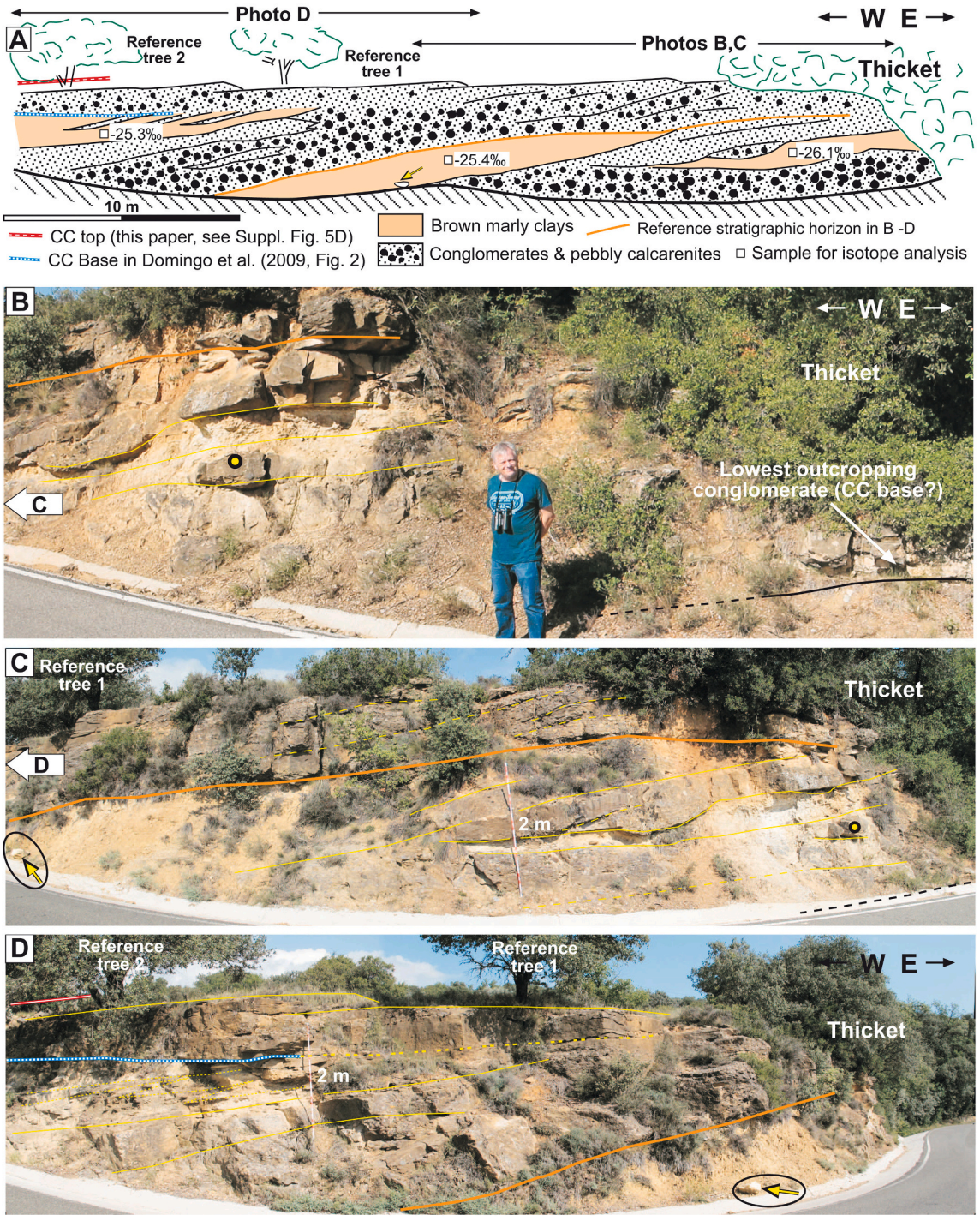

Fig. 8. (A) Sketch of the CC in the Claret road section, drawn from field photos B – D. As the outcrop is situated on a road bend, the perspective of the successive photos is distorted. To alleviate the distortion, two characteristic points are marked in different pictures: a small yellow circle in B and C, and a circled fallen block (arrowed) in A, C and D. The orange line (in the online version) marks the base of the same conglomeratic bed in all pictures. $\delta^{13}C_{org}$ values from marly clays are shown in A. (For interpretation of the references to colour in this figure legend, the reader is referred to the web version of this article.)

the top of the CC is situated about 2 m below the Esplugafreda Formation/Yellowish soil boundary (Fig. 12).

Two sections located close to each other have been studied in the northern part of the Tendrui sector, the T_{DMD} described by DMD (09–19) and one situated in the trench of a dirt tract about 40 m to the north, coded T_{dt} (Fig. 13A). The part of the T_{DMD} section revisited in this study is situated in a small vegetated ravine (Fig. 13A, B; cf., small photo in Fig. 3 of Domingo et al., 2009). It comprises a 20 m thick segment of the Esplugafreda Formation located immediately below the CC, the lowermost part of which is formed by red calcareous mudstones with carbonate nodules, the remainder by brownish silty marls devoid of nodules and gypsum (Fig. 13B, C). DMD (09–19) analyzed about 20 samples from this interval, their values being plotted in Fig. 13C (small diamonds, yellow in the online version). Values of five samples collected for this study (large diamonds, red in the online version, Fig. 13C; Supplementary Table 7) are roughly similar to those of DMD (09–19). While collecting them it was noticed that the marls become increasingly softer and discoloured up to the CC.

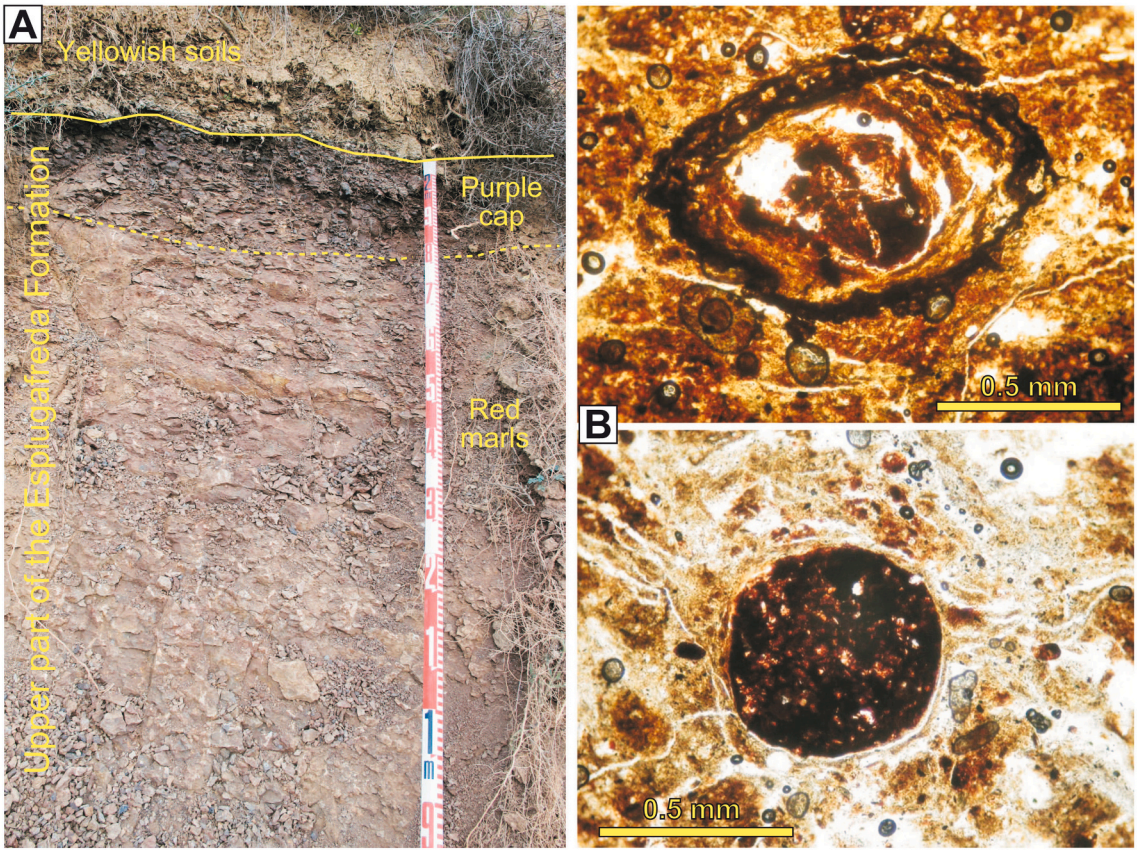

Fig. 9. (A) Close-up of the upper part of the Ad-S section. (B) Micrographs of a thin section of a purple cap sample illustrating two of its numerous ferruginous nodules. (For interpretation of the references to colour in this figure legend, the reader is referred to the web version of this article.)

The nearby T_{dt} section (Fig. 13A) comprised the 8 m thick interval of the Esplugafreda Formation situated just below the CC. Today this section is vegetated only in its upper part, but the excavation of the dirt track trench unearthed numerous subvertical large roots coming down throughout the section from the trees above (Fig. 13D). The section is largely covered by loose clays, but well-indurate grey-brownish silty marls are exposed along several small vertical rills coming down through most of the section, from which six samples were collected (Fig. 13D). The lower five samples were well indurated and gave $\delta^{13}C_{org}$ values ranging from −24.1‰ to −24.8‰, averaging out at 24.4‰ (Fig. 13E; Supplementary Table 8). The uppermost marl sample, collected in the upper vegetated part of the section, was soft and contained numerous traces of recent roots, yielding a $\delta^{13}C_{org}$ value of −25.2‰.

5. Discussion

5.1. Architecture of the Claret Conglomerate

The predominant coarse-grained components of the CC must have been transported by powerful currents, a fact that explains both the erosional base of the unit (Supplementary Fig. 3A) and its encasement in the Esplugafreda Formation (Figs. 2D, 10A, B; 12). Palaeocurrents from cross-bedding and large-scale dunes demonstrate that these currents preferentially flowed to the WSW (Fig. 5A), similar to those indicated by the clast imbrications in the basal conglomerates of the incised valley. This circumstance and the areal concurrence of the incised valley and the CC outcrops suggest that the latter unit was mainly accumulated in a residual depression of the former, which probably explains the lens-like CC shape in the Claret sector (Fig. 2D). Instead, where the CC overlies the Esplugafreda Formation it exhibits a near tabular shape (e.g., Fig. 10B).

The most significant internal architectural features of the CC are observed in the Claret road section. The slope of the low-angle inclined conglomeratic strata coincides with the direction indicated by the palaeocurrents (Fig. 8A). These strata, therefore, must record a forward progradation of the CC during episodes of strong currents. Conversely, silty clays intercalated between the conglomerate strata must have been accumulated in quieter conditions, from which it seems logical to conclude that the progradation of the CC was intermittent, with alternating periods of activity and stillness.

5.2. Onset of the CIE in the study area

Interpretation of $\delta^{13}C_{org}$ results obtained from bulk rocks must be treated with caution, because they may reflect variations in the proportion of autochthonous and allochthonous organic components and/or different degrees of diagenetic degradation. In marine deposits the reliability of $\delta^{13}C_{org}$ curves can be validated (or disproved) through a comparison with other indicators, mainly biostratigraphic data (e.g., Pujalte and Schmitz, 2014; Storme et al., 2012). Such a procedure, however, is more difficult to apply in terrestrial deposits, which are either barren or poorly fossiliferous, as it is the case of the successions here considered. One possible way to circumvent these problems is to analyze high-molecular weight n-alkanes (C_{25} to C_{33}), which have a higher resistance to isotopic exchange (Baczynski et al., 2016). However, even this procedure does not always guarantee accurate results (e.g., Baczynski et al., 2019).

Consequently, the following four criteria have been used in this study to evaluate the significance of the $\delta^{13}C_{org}$ profiles: (1) $\delta^{13}C_{org}$ values from pre-PETM deposits vary between −22 and − 25‰ and those from PETM deposits between −25 and − 27‰, a criterion previously used, for

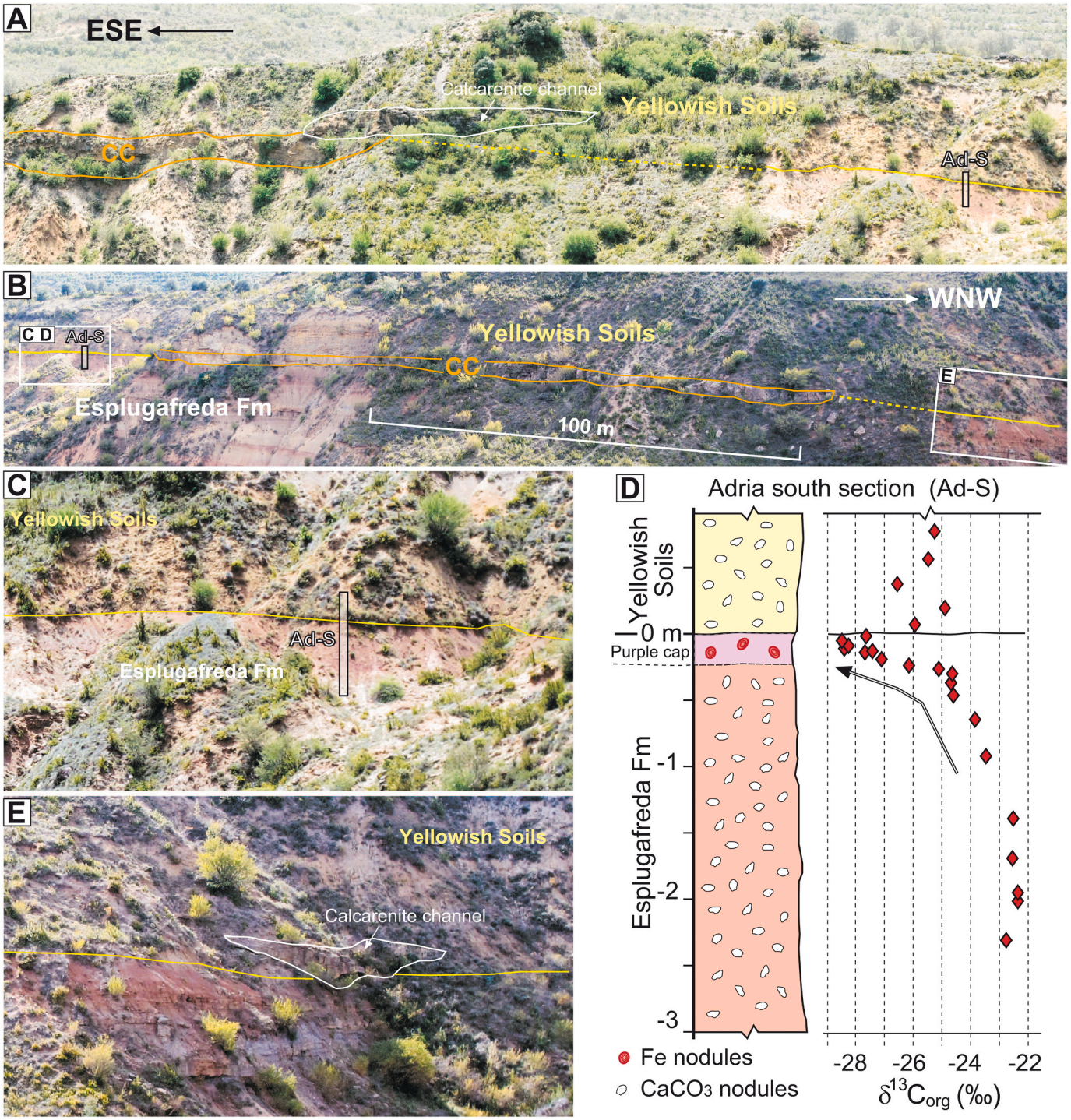

Fig. 10. (A, B) Field views of two adjacent segments of the southern margin of the St Adria valley illustrating the encasement of the CC into the Esplugafreda Formation (location in Fig. 2C). (C) General view of the Ad-S section (location in A and B). (D) $\delta^{13}C_{org}$ isotopic profile of the Ad-S section. (E) Field view of a calcarenite channel with its base party eroding the Esplugafreda Formation (location in B).

instance, by Yans et al. (2014) and Maufrangeas et al. (2020) in sections of the northern Pyrenees; (2) the onset of the CIE entails a *sustained* shift of −2 to −3‰; (3) comparisons between different $\delta^{13}C_{org}$ isotopic profiles of the area, as well as with $\delta^{13}C_{carb}$ profiles when available; (4) last, but not least, field relationships of the studied sections were taken into account.

The isotopic profiles obtained independently by Schmitz and Pujalte (2003) and Manners et al. (2013) in the Esplugafreda section exemplify the application of these criteria (Supplementary Figs. 2B, C). In effect, although respectively based on analyses of carbonate nodules and bulk organic carbon, both studies constrained the PETM to the same interval of the Esplugafreda section, mutually reinforcing their validity. In the latter study, δ^{13}Corg values ranging from −21.5 to −23.5‰ were considered pre-PETM, while those between −24.9 and 26.5‰ were ascribed to the PETM (Supplementary Fig. 2C). Yet, neither Schmitz and Pujalte (2003) nor Manners et al. (2013) gave any significance to short-lived isotopic shifts observed in their respective isotopic profiles of the Esplugafreda Formation (Supplementary Figs. 2B, C).

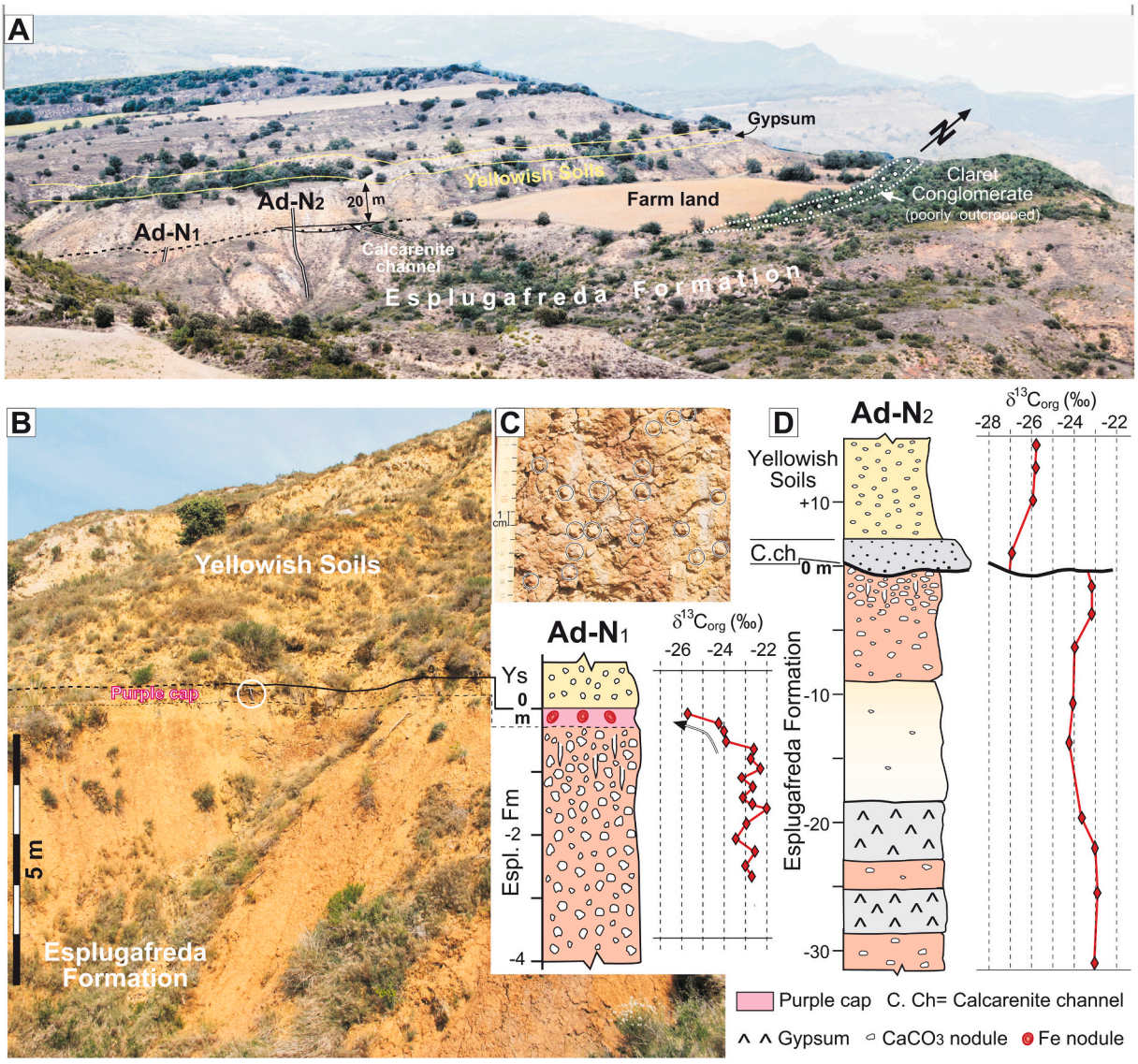

Fig. 11. (A) Field view of the northern margin of the St Adria valley and southern part of the Tendrui sector showing the location of the Ad-N_1 and Ad-N_2 sections, the tree-covered CC of the Tendrui sector and the farm-land situated just above it. (B) Field view and isotope profile of the Ad-N_1 section. The encircled hammer in the photo is situated on the purple cap. (C) Close-up of the Esplugafreda Formation red marls in the Ad-N_1 section showing its numerous $CaCO_3$ soil nodules (some encircled). (D) $\delta^{13}C_{org}$ isotope profile of the Ad-N_2 section. (For interpretation of the references to colour in this figure legend, the reader is referred to the web version of this article.)

An application of the aforementioned criteria in the study area reveals that the isotopic shift most likely associated to the onset of the CIE is the one recorded in the uppermost part of the Esplugafreda section in the Ad-S and Ad-N_1 sections of the St Adria valley (Figs. 10B, 11B). This shift, which is based on high-resolution $\delta^{13}C_{org}$ profiles, is both gradual and persistent, its shape and magnitude (2–4‰) being similar to the one found in terrestrial sections elsewhere (e.g., Baczynski et al., 2013). Finally, this shift is situated in the position predicted in the low resolution $\delta^{13}C_{carb}$ profile reported by the Schmitz and Pujalte (2003) in another section of the St Adria valley (Fig. 2D, Supplementary Fig. 3B).

In the other section studied in this valley (Ad-N_2; Figs. 11D) $\delta^{13}C_{org}$ values from the Esplugafreda Formation provide pre-PETM values (−23 to −24‰), and those of the Yellowish Soils PETM values (−26.1‰ on average). However, the gradual shift which marks the CIE onset in the Ad-S and Ad-N_1 sections is not recorded, a fact readily attributable to the truncation of the top of the Esplugafreda section by a calcarenite channel (Fig. 12B).

Field evidence indicates that the top of the CC in the Tendrui sector is probably situated ≥2 m below the purple horizon capping the Esplugafreda Formation in the adjacent St. Adria sector (Figs. 11A, 12B; Supplementary Fig. 6). Consequently, the CIE onset proposed by DMD (09–19) would be located about 12 m lower than its actual position in the Ad-S and the Ad-N_1 sections (Figs. 12B, 14), which is unrealistic. On top of that, the $\delta^{13}C_{org}$ profile of the T_{DMD} is controversial because of the following facts: (1) average $\delta_{13}C_{org}$ values of the alleged pre-PETM and PETM segments of the Esplugafreda Formation only differ by ~0.7‰ (25.0‰ and 25.7‰, respectively), a shift much smaller than the one expected for the CIE onset; (2) although $\delta_{13}C_{org}$ values lower than −25‰, typical of the PETM, are dominant in the upper 8 m of Esplugafreda Formation, similar values also occur in about half of the samples from the pre-PETM interval; (3) given the proximity of the T_{DMD} and T_{dt} sections (Fig. 13A), $\delta_{13}C_{org}$ values of their supposed PETM intervals should be similar but they do differ by −1.1‰ on average, and the values of the latter (−24 to −25.2‰) match those of the pre-PETM segment of the former (Fig. 13C, E and Fig. 14).

The reason why $\delta^{13}C_{org}$ values from the upper part of the

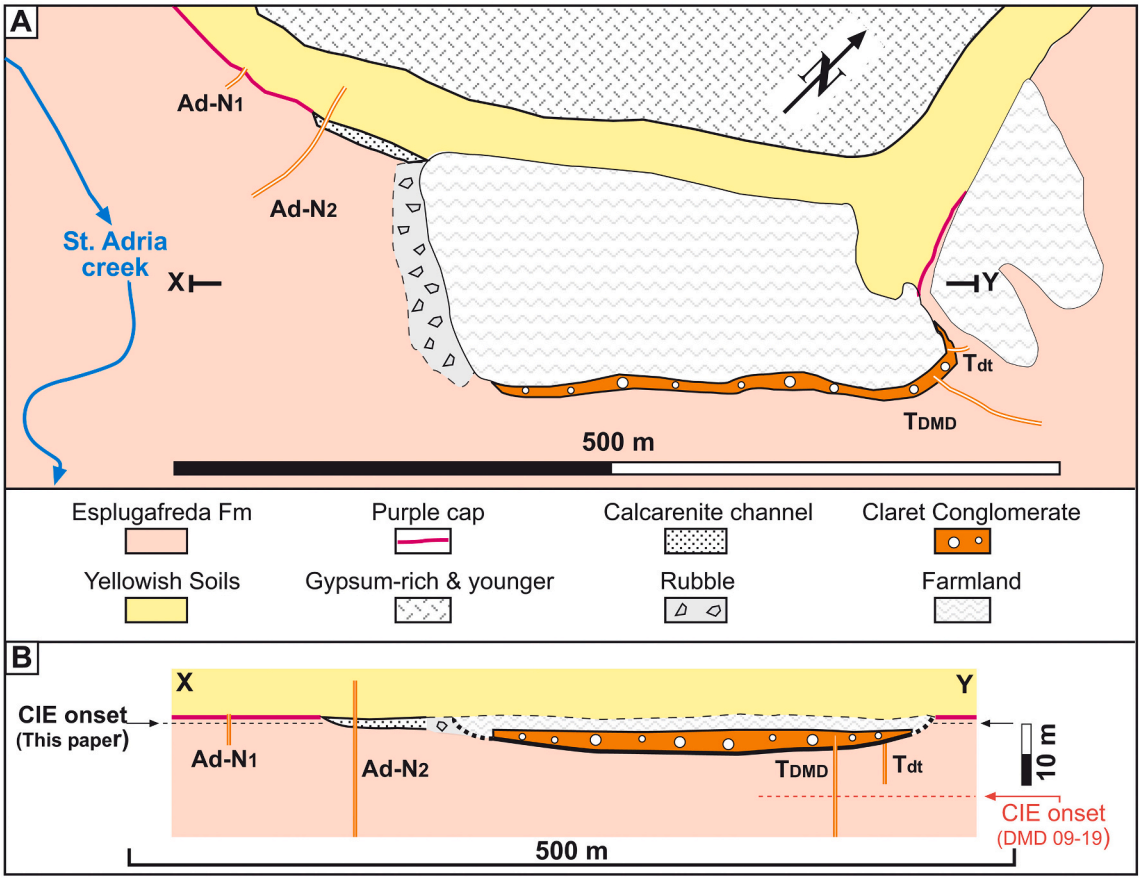

Fig. 12. (A) Outcrop map of the Paleocene-Eocene boundary interval units in the Tendrui sector. (B) Cross-section projected across the X-Y line; note that vertical scale is exaggerated. Locations of the CIE onset according to DMD (09–19) and this paper are indicated. Explanation within the text.

Esplugafreda Formation in the T_{DMD} and Tdt sections are lower than in coeval deposits of the St Adria valley still needs to be investigated. One possibility is that sediments from the T_{DMD} section contain a high proportion of resedimented fossil carbon depleted in ^{13}C. In that case, however, the isotopic composition of the 8 m interval of the Esplugafreda Formation situated below the CC in the T_{DMD} and T_{dt} sections should be similar, which is not the case. Whatever the reason, the above facts strongly suggest that the $\delta^{13}C_{org}$ profiles of the T_{DMD} and T_{dt} sections do not faithfully record the global trend and, consequently, are not well suited to fix the position of the CIE onset.

In the Claret sector the marked erosional character of the base of the CC (Supplementary Fig. 3A) suggests also an encasement of the unit, but the total amount of the erosion into the underlying deposits cannot be quantified. Therefore, the possible preservation of the CIE onset in this sector can only be appraised through an inspection of continuous isotopic profiles. Such an inspection cannot be carried out in the Claret road section, since no samples can be retrieved from the 2-m-thick covered interval below the CC (Figs. 7, 8, 14).

The Claret north and Claret hamlet sections, in which the boundary between the incised valley fill and the CC is well exposed, offer a better chance to locate the CIE onset (Figs. 6, 14). In the former, pre-PETM $\delta^{13}C_{org}$ values (−22.0 to −22.9‰) persist in the grey calcarenites and marls until 20 cm below the CC base, where a single value of −25.2‰ was obtained (Figs. 6A, 13). Should it mark the base of the CIE isotope shift, the PETM onset would be situated just about 20 cm below the CC. However, the return to less negative $\delta^{13}C_{org}$ values higher up (−24.2 to −22.3‰) argues against the −25.2‰ value as the initiation of a persistent shift. Alternatively, this very negative value might be attributed to the recent alteration observable in the sediments situated immediately below the CC. As shown in Supplementary Fig. 3A, in effect, parts of the sediments situated 20 cm or less below the CC are disaggregated and their stratification is blurred, clear signs of alteration caused probably by waters percolating through the CC. The $\delta^{13}C$ values of the four samples from these 20 cm vary between −23.1‰ and −25.3‰, whereas those of ten samples collected from unaltered sediments between 28 and 190 cm below the CC vary between −21.7‰ and −22.7‰ (Supplementary Table 1).

As explained before, the red mudstones of the Claret hamlet section are thought to record the final infilling of the incised valley. If this interpretation proves correct, they post-date the grey calcarenites and marls of the Claret north section. The four samples analyzed from these red mudstones provided pre-PETM $\delta^{13}C_{org}$ values, from −24.4 to −23.9‰ (−24.1‰ on average; Figs. 6B and 13). The $\delta^{13}C_{carb}$ values reported by Pujalte et al. (2009) from three calcareous soil nodules from these red mudstones are also clearly pre-PETM (−7.5‰; Supplementary Fig. 3B). Therefore, no clear evidence of the CIE onset can be discerned in any of the sections of the Claret sector.

5.3. Sedimentary response to the PETM hydrological change

Given that the development of extensive alluvial accumulations cannot be instantaneous, some time must have elapsed from the onset of the PETM hydrological change to the arrival of CC gravels and Yellowish Soils sediments to the study area, as further demonstrated by the progradacional character of the CC. The duration of the delay was quantified by DMD (09–19) in 9–16 kyr in the Claret road section and in 13–24 kyr in the T_{DMD} section, based on the position of the CIE onset assumed in each of them. However, according to the data discussed above, their assumption has been proven incorrect in the former section and is highly uncertain in the latter.

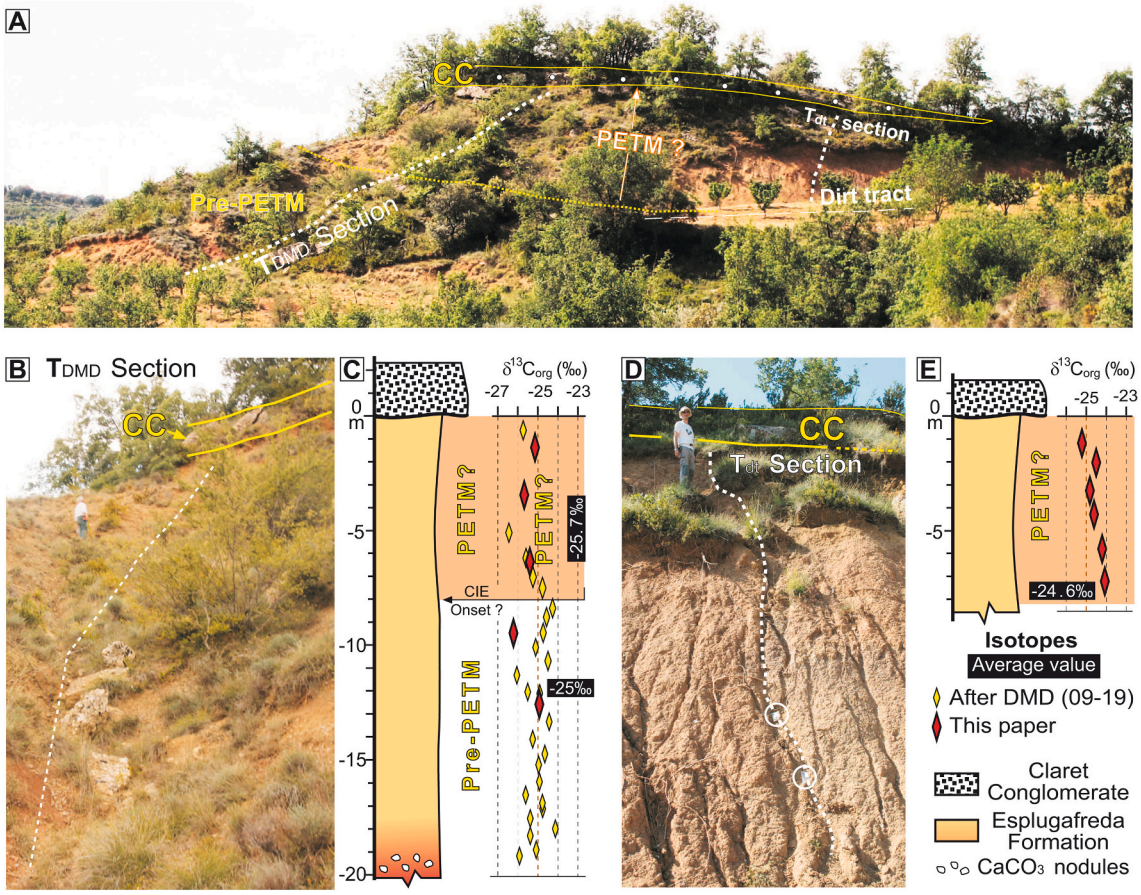

Fig. 13. (A) Field view of the northern part of the Tendrui sector with location of the T_{DMD} and the T_{dt} sections. Note abundant vegetation. (B, C) Field view and isotope profile of the T_{DMD} section. (D, E) Field view and isotope profile of the T_{dt} section.

The information obtained in this study offers the possibility to circumvent these two problematic sections by focusing on the base of the Yellowish Soils in the sections in which the CC is absent, rather than on the CC itself. In effect, based on Walther's Law of Facies, it is reasonable to assume that the first Yellowish marls reached the study area at approximately the same time as the CC, if not before.

The Ad-S and Ad-N_1 sections provide sound evidence that the onset of the CIE is situated ~1 m below the base of the Yellowish Soils (Figs. 10D, 11B, 12). The length of this interval cannot be calculated with available methods and, therefore, it has been tentatively estimated by assuming the same sedimentation rate as across the PETM onset and core. This procedure, although admittedly inexact, has the advantage of permitting a direct comparison with the estimates of DMD (09–19).

The duration of the PETM onset and core was calculated to be 80 kyr by Bowen et al. (2004) and Röhl et al. (2007). In the Ad-S and Ad-N1 sections the onset and core of the PETM are represented by the topmost 1 m of the Esplugafreda Formation plus the 20 m thick Yellowish Soils. Their 21 m cumulative thickness (compacted), therefore, implies an average sedimentation rate of 26.25 cm kry^{-1}. Consequently, the 1 m thick segment of the PETM onset preceding the arrival of the first Yellowish marls to the study area might represent ~3.8 kyr, less than half of the lowest estimate of DMD (09–19) and about one sixth of their highest one.

Since the source area of the Garumnian alluvium was situated about 15 km to the north-east from the study area (Supplementary Fig. 1) this figure entails an averaged expansion rate of the extensive PETM depositional system of about 4 km/kyr. It is unlikely, however, that such expansion rate was uniform throughout the ~3.8 kyr lag time, since the shape of the initial isotope excursion clearly indicates a gradual increment of light carbon (Figs. 10D, 11B) and because the climate response to warming is slightly delayed (Zeebe et al., 2016). Also, both the temperature rise and the concomitant increase of extreme rainfall episodes during the ongoing anthropogenic warming of the Earth are being gradual (Shukla and Sen, 2021). Similar gradual increases, therefore, may have occurred during the onset of the PETM. Consequently, it is to be expected that the sedimentary expansion rate of the PETM alluvial system, which may have been slow at first, progressively accelerated in parallel with the CO_2 increment and the intensification of the warming. Whatever the case, the response of the sedimentary system to the PETM hydrological change seems to have been, in geological terms, comparatively rapid.

6. Conclusions

The claim that the sedimentary response to the PETM hydrological change in the south Pyrenean Tremp-Graus Basin was delayed by 16.5 ± 7.5 kyr is challenged with new field and organic carbon isotope data. This claim was based on the assertion that the onset of the CIE was recorded 3 and 8 m below the CC in the Claret and Tendrui sections. However, new field data and organic carbon isotopic analyses of one hundred samples from eight sections, including the two conflicting ones, lead to a different conclusion. Field mapping and observations demonstrate that at Claret, Tendrui and elsewhere in the study area, the CC is partly or totally erosively encased within the underlying deposits and is laterally discontinuous. In the two sections coded Ad-S and Ad-N_1, in which the CC is absent and the Yellowish Soils conformably rest on the Esplugafreda Formation, the onset of the CIE has been confidently pinpointed about 1 m below the base of the Yellowish Soils. This onset, however, is truncated by the CC erosional base at the Claret and Tendrui sections, making them unsuitable for any chronological reconstructions.

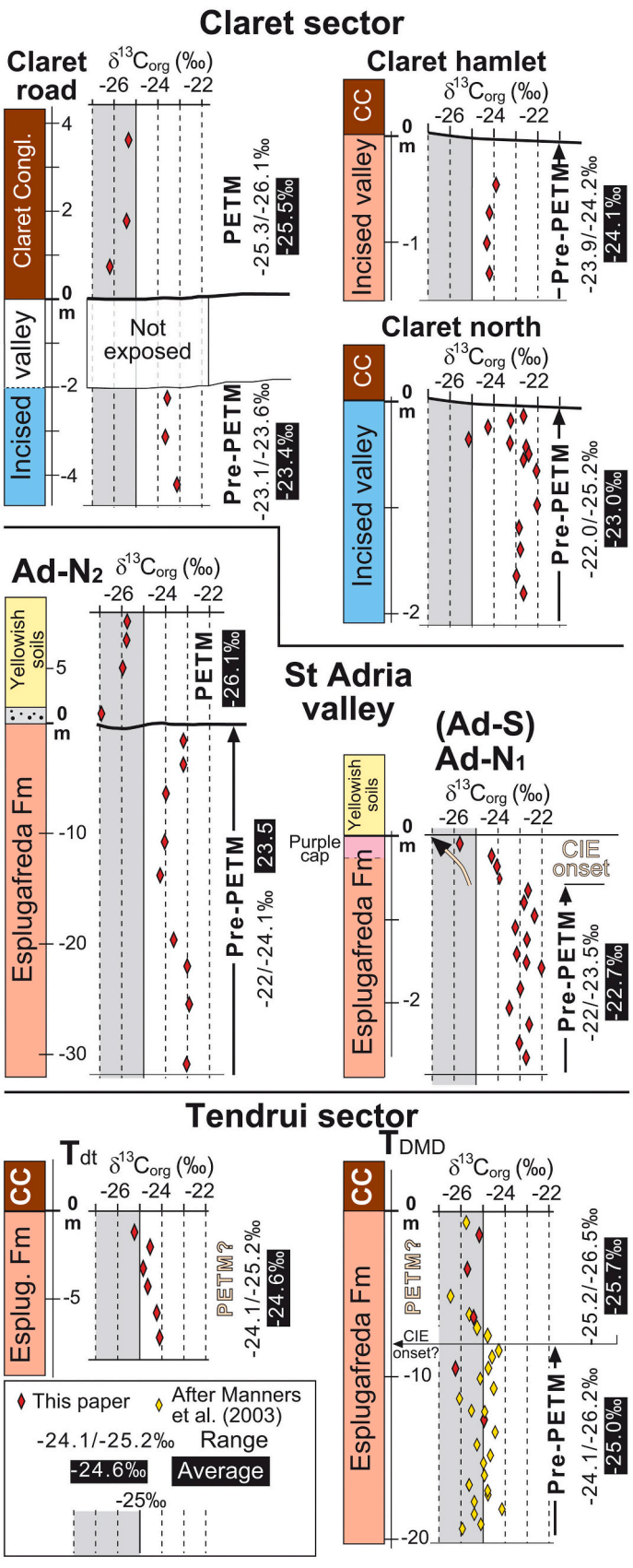

Fig. 14. Organic carbon isotope profiles from the P-E boundary sections analyzed in this study. Note that values of the T_{DMD} section are at odds with those of the other sections. Explanation within the text.

As the expansion of alluvial systems cannot be instantaneous, some time must have elapsed between the onset of the hydrological change and the arrival of PETM alluvium to the study area. In fact, the internal architecture of the CC, indicative of intermittent progradation, requires a progressive development. A tentative estimate, based on sedimentation rates, suggests that the arrival of PETM alluvium to the Claret-Tendrui area occurred ~3.8 kyr after the onset of the CIE, about a third of the lowest estimate of previous authors. Since the study area was situated about 15 km from the source area, this new estimate entails a minimum expansion rate of about 4 km kyr^{1} and supports a rapid environmental response of the sedimentary system to the PETM hydrological change.

Declaration of Competing Interest

The authors declare that they have no known competing financial interests or personal relationships that could have influenced the research reported in this paper.

Acknowledgements

Research by VP and AP was supported by MINECO/MCI/FEDER-UE projects CGL2015-65404-R and PID2019-105670GB-I00/AEI/10.13039/501100011033 of the Spanish Government, and by the Consolidated Research Group IT930-16 of the Basque Government. Research by BS was supported by the Swedish Research Council. Comments by two anonymous reviewers and editors Thomas Algeo and Alex Dickson helped to improve the original manuscript.

Appendix A. Supplementary data

Supplementary data to this article can be found online at https://doi.org/10.1016/j.palaeo.2021.110818.

References

Allen, P.A., 2017. The Sediment Routing Systems: The Fate of Sediments from Source to Sink. Cambridge University Press (403 pp.).

Armitage, J.J., Duller, R.A., Whittaker, A.C., Allen, P.A., 2011. Transformation of tectonic and climatic signals from source to sedimentary archive. Nat. Geosci. 4, 231–235. https://doi.org/10.1038/ngeo1087.

Armitage, J.J., Dunkley Jones, T., Duller, R.A., Whittaker, A.C., Allen, P.A., 2013. Temporal buffering of climate-driven sediment flux cycles by transient catchment response. Earth Planet. Sci. Lett. 369–370, 200–210. https://doi.org/10.1016/j.epsl.2013.03.020.

Baceta, J., Pujalte, V., Wright, V.P., Schmitz, B., 2011. Carbonate platform models, sea-level changes and extreme climatic events during the Paleocene-early Eocene greenhouse interval: a basin-platform-coastal plain transect across the southern Pyrenean basin. In: Pree-meeting Field trips Guidebook, 28th IAS meeting. Zaragoza (C. Arenas, L. Pomar and F. Colombo, Eds.). Sociedad Geológica de España, Geo-Guías, 7, pp. 151–198.

Baczynski, A.A., McInerney, F.A., Wing, S.L., Kraus, M.J., Bloch, J.I., Boyer, D.M., Secord, R., Morse, P.E., Fricke, H.C., 2013. Chemostratigraphic implications of spatial variation in the Paleocene-Eocene thermal Maximum carbon isotope excursion, SE Bighorn Basin, Wyoming. Geochem. Geophys. 14, 4133–4152. https://doi.org/10.1002/ggge.20265.

Baczynski, A.A., McInerney, F.A., Wing, S.L., Kraus, M.J., Morse, P.E., Bloch, J.I., Chung, A.H., Freeman, K.H., 2016. Distortion of carbon isotope excursion in bulk soil organic matter during the Paleocene-Eocene thermal maximum. GSA Bull. 128, 1352–1366. https://doi.org/10.1130/B31389.1.

Baczynski, A.A., McInerney, F.A., Freeman, K.H., Wing, S.L., the Bighorn Basin Coring Project (BBCP) Science Team, 2019. Carbon isotope record of trace n-alkanes in a continental PETM section recovered by the Bighorn Basin Coring Project (BBCP). Paleoceanography and Paleoclimatology 34, 1–13. https://doi.org/10.1029/2019PA003579.

Bowen, G.J., Beerling, D.J., Koch, P.L., Zachos, J.C., Quattlebaum, T., 2004. A humid climate state during the Palaeocene-Eocene thermal maximum. Nature 432, 495–499. https://doi.org/10.1038/nature03115.

Capel Molina, J., 1974. Génesis de las inundaciones de Octubre de 1973 en el Sureste de la Península Ibérica. Cuad. Geog. 4, 140–166.

Carmichael, M.J., Inglis, G.N., Badger, M.P.S., Naafs, D.A., Behrooza, L., Remmelzwaal, S., Monteiro, F.M., Rohrssen, M., Farnsworth, A., Buss, H.L., Dickson, A.J., Valdes, P.J., Lunt, D.J., Pancost, R.D., 2017. Hydrological and associated biogeochemical consequences of rapid global warming during the Paleocene-Eocene thermal Maximum. Gloplacha 157, 114–138. https://doi.org/10.1016/j.gloplacha.2017.07.014.

Carmichael, M.J., Pancost, R.D., Lunt, D.J., 2018. Changes in the occurrence of extreme precipitation events at the Paleocene–Eocene thermal maximum. Earth Planet. Sci. Lett. 501, 24–36. https://doi.org/10.1016/j.epsl.2018.08.005.

Colombera, L., Arévalo, O.J., Mountney, N.P., 2017. Fluvial-system response to climate change: the Paleocene-Eocene Tremp Group, Pyrenees, Spain. Gloplacha 157, 1–17. https://doi.org/10.1016/j.gloplacha.2017.08.011.

Cuevas, J.L., 1992. Estratigrafía del "Garumniense" de la Conca de Tremp. Prepirineo de Lérida. Acta Geol. Hisp. 27, 95–108.

Deser, C., Lehner, F., Rodgers, K.B., Ault, T., Delworth, T.L., DiNezio, P.N., Fiore, A., Frankignoul, C., Fyfe, J.C., Horton, D.E., Kay, J.E., Knutti, R., Lovenduski, N.S., Marotzke, J., McKinnon, K.A., Minobe, S., Randerson, J., Screen, J.A., Simpson, I.R., Ting, M., 2020. Insights from Earth system model initial-condition large ensembles and future prospects. Nat. Clim. Chang. 10, 277–286. https://doi.org/10.1038/s41558-020-0731-2.

Domingo, L., López-Martínez, N., Leng, M.J., Grimes, S.T., 2009. The Paleocene–Eocene Thermal Maximum record in the organic matter of the Claret and Tendruy continental sections (South-central Pyrenees, Lleida, Spain). Earth Planet. Sci. Lett. 281, 226–237. https://doi.org/10.1016/j.epsl.2009.02.025.

Duller, R.A., Armitage, J.J., Manners, H.R., Grimes, S., Dunkley Jones, J., 2019. Delayed sedimentary response to abrupt climate change at the Paleocene-Eocene boundary, northern Spain. Geology 47, 159–162. https://doi.org/10.1130/G45631.1.

Foreman, B.Z., 2014. Climate-driven generation of a fluvial sheet sand body at the Paleocene-Eocene boundary in north-West Wyoming (USA). Basin Res. 26, 225–241. https://doi.org/10.1111/bre.12027.

Foreman, B.Z., Heller, P.L., Clementz, M.T., 2012. Fluvial response to abrupt global warming at the Palaeocene/Eocene boundary. Nature 491, 92–95. https://doi.org/10.1038/nature11513.

García Veigas, J., 1997. First Continental Evaporitic phase in the South Pyrenean Central Area: Tremp Gypsum (Garumn Facies, Upper Paleocene; Allochtonous Zone). In: Busson, G., Schreiber, B.Ch. (Eds.), Sedimentary Deposition in Rift and Foreland Basins in France and Spain (Paleogene and Lower Neogene). Columbia University Press, pp. 335–342.

Gibson, T.G., Bybell, L.M., Mason, D.B., 2000. Stratigraphic and climatic implications of clay mineral changes around the Paleocene/Eocene boundary of the northeastern US margin. Sedim. Geol. 134, 65–92. https://doi.org/10.1016/S0037-0738(00)00014-2.

Handley, L., O'Halloran, A., Pearson, P.N., Hawkins, E., Nicholas, C.J., Schouten, S., McMillan, I.K., Pancost, R.D., 2012. Changes in the hydrological cycle in trop-ical East Africa during the Paleocene-Eocene Thermal Maximum. Palaeogeogr. Palaeoclimatol. Palaeoecol. 329, 10–21. https://doi.org/10.1016/j.palaeo.2012.02.002.

Held, I.M., Soden, B.J., 2006. Robust responses of the Hydrological Cycle to Global Warming. J. Clim. 19, 5686–5699. https://doi.org/10.1175/JCLI3990.1.

Jiang, J., Hu, X., Li, J., BouDagher-Fadel, M., Garzanti, E., 2021. Enhanced hydrological change during the Paleocene-Eocene thermal maximum (PETM) recorded in shallow-marine Xigaze forearc basin (southern Tibet). Palaeogeogr. Palaeoclimatol. Palaeoecol. 562 (2021), 110095 https://doi.org/10.1016/j.palaeo.2020.110095.

John, C.M., Bohaty, S.M., Zachos, J.C., Sluijs, A., Gibbs, S., Brinkhuis, H., Bralower, T.J., 2008. North American continental margin records of the Paleocene–Eocene thermal maximum: implications for global carbon and hydrological cycling. Paleoceanography 23, PA2217. https://doi.org/10.1029/2007PA001465.

Klappa, C.F., 1978. Biolithogenesis of *Microcodium*: elucidation. Sedimentology 25, 489–522.

Koch, P.L., Zachos, J.C., Gingerich, P.D., 1992. Correlation between isotope records in marine and continental carbon reservoirs near the Paleocene/Eocene boundary. Nature 358, 319–322.

Košir, A., 2004. *Microcodium* revisited: root calcification products of terrestrial plants on carbonate-rich substrates. J. Sediment. Res. 74, 845–857. https://doi.org/10.1306/040404740845.

Kraus, M.J., McInerney, F.A., Wing, S.L., Secord, R., Baczynski, A.A., Bloch, J.I., 2013. Paleohydrologic response to continental warming during the Paleocene–Eocene Thermal Maximum, Bighorn Basin, Wyoming. Palaeogeogr. Palaeoclimatol. Palaeoecol. 370, 196–208. https://doi.org/10.1016/j.palaeo.2012.12.008.

Kraus, M.J., Woody, D.T., Smith, J.J., Dukic, V., 2015. Alluvial response to the Paleocene–Eocene Thermal Maximum climatic event, Polecat Bench, Wyoming (U.S.A.). Palaeogeogr. Palaeoclimatol. Palaeoecol. 435, 177–192. https://doi.org/10.1016/j.palaeo.2015.06.021.

Manners, H.R., Grimes, S.T., Sutton, P.A., Domingo, L., Leng, M.J., Twitchett, R.J., Hart, M.B., Dunkley Jones, T., Pancost, R.D., Duller, R., Lopez-Martinez, N., 2013. Magnitude and profile of organic carbon isotope records from the Paleocene–EoceneThermal Maximum: evidence from northern Spain. Earth Planet. Sci. Lett. 376, 220–230. https://doi.org/10.1016/j.epsl.2013.06.016.

Maufrangeas, A., Leleu, S., Loisy, C., Roperch, P., Jolley, D., Vinciguerra, C., Nguyen-Thuyet, O., 2020. Stratigraphy of the Paleocene continental sedimentary succession of the northern Pyrenean basin (Corbières, southern France) using $\delta^{13}C_{org}$ isotopes. J. Geol. Soc. Lond. 177, 752–765. https://doi.org/10.1144/jgs2019-084.

McInerney, F.A., Wing, S.L., 2011. The Paleocene Eocene ThermalMaximum: a perturbation of carbon cycle, climate, and biosphere with implications for the future. Annu. Rev. Earth Planet. Sci. 39, 489–516. https://doi.org/10.1146/annurev-earth-040610-133431.

Minelli, N., Manzi, V., Roveri, M., 2013. The record of the Paleocene-Eocene thermal maximum in the Ager Basin (Central Pyrenees, Spain). Geol. Acta 11, 421–441. https://doi.org/10.1344/105.000002061.

Pancost, R.D., 2017. Climate change narratives. Nat. Geosci. 10, 466–468.

Payros, A., Pujalte, V., Orue-Etxebarria, X., Apellaniz, E., Bernaola, G., Baceta, J.I., Caballero, F., Dinarés-Turell, J., Monechi, S., Ortiz, S., Schmitz, B., Tosquella, J., 2016. In: Montenari, M. (Ed.), The Relevance of Iberian Sedimentary Successions for Paleogene Stratigraphy and Timescales. Stratigraphy & Timescales, pp. 393–489.

Plink-Björklund, P., Birgeneier, L., Jones, E., 2014. Extremely bad early Eocene weather: evidence for extreme precipitation from rived deposits. Rendiconti Online della Soc. Geol. It. 31, 175–176. https://doi.org/10.3301/ROL.2014.107.

Pujalte, V., Schmitz, B., 2005. Revisión de la estratigrafía del Grupo Tremp ("Garumniense", Cuenca de Tremp-Graus, Pirineos meridionales). Geogaceta 38, 79–82.

Pujalte, V., Schmitz, B., 2014. Comment on "Magnitude and profile of organic carbon isotope records from the Paleocene–Eocene Thermal Maximum: evidence from northern Spain" by Manners et al. [Earth Planet. Sci. Lett. 376 (2013) 220–230]. Earth Planet. Sci. Lett. 395, 291–293. https://doi.org/10.1016/j.epsl.2014.03.054.

Pujalte, V., Schmitz, B., 2019. Record of the Paleocene–Eocene Thermal Maximum in the Southern and Western Pyrenees. In: Quesada, C., Oliveira, J.T. (Eds.), The Geology of Iberia: A Geodynamic Approach, Springer Nature Switzerland AG, pp. 13–17. https://doi.org/10.1007/978-3-030-11190-8_2.

Pujalte, V., Baceta, J.I., Schmitz, B., Orue-Etxebarria, X., Payros, A., Bernaola, G., Apellaniz, E., Caballero, F., Serra-Kiel, J., Tosquella, J., 2009. Redefinition of the Ilerdian Stage (early Eocene). Geol. Acta 7, 177–194. https://doi.org/10.1344/105.000000268.

Pujalte, V., Schmitz, B., Baceta, J.I., 2014. Sea-level changes across the Paleocene–Eocene interval in the Spanish Pyrenees, and their possible relationship with North Atlantic magmatism. Palaeogeogr. Palaeoclimatol. Palaeoecol. 393, 45–60. https://doi.org/10.1016/j.palaeo.2013.10.016.

Pujalte, V., Robador, A., A., Samsó, J.Mª., 2016. A siliciclastic braid delta within a lower Paleogene carbonate platform (Ordesa-Monte Perdido National Park, southern Pyrenees, Spain): Record of the Paleocene–Eocene Thermal Maximum perturbation. Palaeogeogr. Palaeoclimatol. Palaeoecol. 459, 453–470. https://doi.org/10.1016/j.palaeo.2016.07.029.

Röhl, U., Westerhold, T., Bralower, T.J., Zachos, J.C., 2007. On the duration of the Paleocene- Eocene thermal Maximum (PETM). Geochem. Geophys. Geosyst. 8, 1–13. https://doi.org/10.1029/2007GC001784.

Rosell, J., Linares, R., Llompart, C., 2001. El "Garumniense" prepirenaico. Rev. Soc. Geol. Esp. 14, 47–56.

Schmitz, B., Pujalte, V., 2003. Sea-level, humidity, and land-erosion records across the initial Eocene thermal maximum from a continental-marine transect in northern Spain. Geology 31, 689–692. https://doi.org/10.1130/G19527.1.

Schmitz, B., Pujalte, V., 2007. Abrupt increase in seasonal extreme precipitation at the Paleocene-Eocene boundary. Geology 35, 215–218. https://doi.org/10.1130/G23261A.1.

Schmitz, B., Pujalte, V., Núñez-Betelu, K., 2001. Climate and sea-level perturbations during the Incipient Eocene thermal Maximum: evidence from siliciclastic units in the Basque Basin (Ermua, Zumaia and Trabakua Pass), northern Spain. Palaeogeogr. Palaeoclimatol. Palaeoecol. 165, 299–320. https://doi.org/10.1016/S0031-0182(00)00167-X.

Shukla, T., Sen, I.S., 2021. Preparing for floods on the Third Pole. Science 372, 232–234. https://doi.org/10.1126/science.abh3558.

Simpson, G., Castelltort, S., 2012. Model shows that rivers transmit high-frequency climate cycles to the sedimentary record. Geology 40, 1131–1134. https://doi.org/10.1130/G33513.1.

Slotnick, B.S., Dickens, G.R., Nicolo, M.J., Hollis, C.J., Crampton, J.S., Zachos, J.C., Sluijs, A., 2012. Large-amplitude variations in carbon cycling and terrestrial weathering during the latest Paleocene and Earliest Eocene: the record at Mead Stream, New Zealand. J. Geol 120, 487–505. https://doi.org/10.1086/666743.

Sluijs, A., Bowen, G.J., Brinkhuis, H.L., Lourens, J., Thomas, E., 2007. The Palaeocene–Eocene ThermalMaximum super greenhouse: biotic and geochemical signatures, age models and mechanisms of global change. In: Williams, M., Haywood, A.M., Gregory, F.J., Schmidt, D.N. (Eds.), Deep-Time Perspectives on Climate Change:Marrying the Signal from Computer Models and Biological Proxies. Special Publications, The Geological Society, London, The Micropalaeontological Society, pp. 323–349.

Storme, J.-Y., Devleeschouwer, X., Schnyder, J., Cambier, G., Baceta, J.I., Pujalte, V., Di Matteo, A., Iacumin, P., Yans, J., 2012. The Palaeocene/Eocene boundary section at Zumaia (Basque-Cantabric Basin) revisited: new insights from high-resolution magnetic susceptibility and carbon isotope chemostratigraphy on organic matter ($\delta^{13}C_{org}$). Terra Nova 24, 310–317. https://doi.org/10.1111/j.1365-3121.2012.01064.x.

Yans, J., Marandat, B., Masure, E., Serra-Kiel, J., Schnyder, J., Storme, J.-Y., Marivaux, L., Adnet, S., Vianey-Liaud, M., Rodolphe Tabuce, R., 2014. Refined bio-(benthic foraminifera, dinoflagellate cysts) and chemostratigraphy ($\delta^{13}C_{org}$) of the earliest Eocene at Albas-Le Clot (Corbières, France): implications for mammalian biochronology in Southern Europe. Newsl. Stratigr. 47, 331–353. https://doi.org/10.1127/nos/2014/0050.

Zachos, J.C., Dickens, G.R., Zeebe, R.E., 2008. An early Cenozoic perspective on greenhouse warming and carbon-cycle dynamics. Nature 451, 279–283. https://doi.org/10.1038/nature06588.

Zeebe, R.E., Ridgwell, A., Zachos, J.C., 2016. Anthropogenic carbon release rate unprecedented during the past 66 million years. Nat. Geosci. 9, 325–329. https://doi.org/10.1038/NGEO2681.